KTH Engineering Sciences

SPATIAL MODE ENGINEERING IN MID-INFRARED OPTICAL PARAMETRIC OSCILLATORS

Charlotte Liljestrand

Master of Science Thesis

Laser Physics
Department of Applied Physics
School of Engineering Science
Royal Institute of Technology

Stockholm, Sweden 2011

TRITA-FYS 2011:39

ISSN 0280-316X

ISRN KTH/FYS/--11:39-SE

Till Mormor

Abstract

The purpose of this thesis was to investigate the possibilities of enhancing the temporal and spatial coherence of parametric devices in the mid-infrared spectrum by exploiting inherent coherence selection of Bessel beams. Several optical parametric oscillators (OPO) were constructed and characterized for various types of resonators and pump lasers.

In the first part of this work an OPO was constructed out of a periodically poled KTP (PPKTP) crystal within a stable resonator. It was pumped by a Q-switched Nd:YAG laser in transversal and longitudinal single mode operation. The OPO was pumped at 1064 nm and operated at signal wavelength of 1595.9 nm with a bandwidth at FWHM of 0.2 nm and idler wavelength 3192.9 nm and bandwidth of 0.5nm at FWHM. The stable resonator was constructed out of a curved input coupler and a planar output coupler to generate a spatially coherent beam. The beam quality factor of the OPO was measured to M^2=1.3 and M^2=1.7 in the horizontal and the vertical direction respectively.

In the second part of this work conical beams, and hence noncollinear phase matching, was used. This was done to improve and study the temporal and spatial coherence of the generated beam if the OPO is pumped by a laser operating in multiple transversal and longitudinal modes. Using noncollinear phase matching provides a possibility of generating a highly coherent signal (or idler) wave when using a pump laser which operates in multiple transversal and longitudinal modes. Usually, such pump laser makes it difficult to generate highly coherent beams since the properties, such as bandwidth and beam quality factor, of the pump laser are transferred to the generated waves. So called multimode lasers, which operate in multiple modes, can be considered inexpensive and reliable while providing high pulse energies, and they are therefore attractive as pump sources for nonlinear processes. Throughout this second part a Q-switched Nd:YAG laser operating in multiple transversal and longitudinal modes at a wavelength 1064 nm was used. Optical parametric generation (OPG) was used to compare the effects between pumping with a Gaussian wave, and collinear phase matching, and pumping with a conical, a Bessel beam and hence noncollinear phase matching. Thereafter, optical parametric oscillation was studied with collinear and noncollinear phase matching using a Fabry-Perot cavity. The OPO pumped by a Q-switched Gaussian beam, and hence using collinear phase matching had a signal wave at 1596.3 nm and a bandwidth at FWHM of 4 nm. The OPO pumped by a conical beam, hence a Bessel beam and noncollinear phase matching, had a signal wave at 1596.5 nm and a bandwidth at FWHM of 0.2 nm. Both OPOs had a beam quality factor M^2~2 in horizontal and vertical direction.

Acknowledgements

First of all I would like to thank my supervisor Nicky Thilmann. Thank you for teaching me skills in the lab, providing me with a lot of knowledge and feedback not only about my work but other interesting topics, too. Also, for helping me out when nothing seemed to be working and the lasers refused to start and I started to go crazy, and for laughing at me when I got excited over the experiments in the lab. And thank you, for a lot of laughters and good times while working in the lab.

I would like to thank Prof. Valdas Pasiskevicius, not only for offering me the opportunity to do this thesis work, but also for introducing me for the amazing, fascinating subject of nonlinear optics and laser physics, and helping me find the passion for science, research and nonlinear technology. Thank you, for sharing your wisdom and endless knowledge, and for hooking me out there in the beautiful corridor of Alba Nova.

I am grateful to Andrius Zukauskas, who supplied the PPKTP crystals I used in this work. Thank you for sharing your enthusiasm and knowledge of these crystals, and for happily answering my questions both inside and outside the lab, and for, together with Nicky, letting me take part in some fascinating experiments and a lot of good times. You have opened up a new fascinating world of science for me.

To Hoon Jang, with whom I have spent numerous long nights in the lab, a lot of portions of great sushi and many fruitful discussions, I would really like to say special thanks. Thank you for your great company, friendship and all the times you have helped me with everything from Matlab code to just being a good, intelligent friend.

Michele Manzo, Thank you for being one of my best friends, for sharing office, so many laughters and discussions about physics, science and life, at and outside of work with me. You are always happy to share your knowledge in electronics, photonic crystals, Italian cooking, the wonderful language of Italy and life over all. Thank you for always being there for me, you are a wonderful friend. I am convinced you will be able to use your Lithium Niobate crystals to take over the world.

I would also like to thank Staffan Tjörnhammar, Ashraf Mohamedelhassan and Michael Arens for sharing office with me, for a lot of laughters and great discussions, for a lot of help when my mind got stuck, for sharing my fascination, and for reminding me to eat dinner and sleep. A special thanks to Staffan, whom helped me out a lot and supported me enormously in the end of the thesis work when my energy was starting to fade.

To Kai Seger, Martin Levenius and Niels Meiser, thank you for all the games of Magic and fun and interesting discussions during lunch time and outside of work.

I am so grateful to all the members in Laser physics research group for always happily sharing their knowledge, their willingness to give a helping hand at any occasion, and for making me feel so welcome in the group. You are the best colleagues one can wish for. It has been wonderful in so many ways to work with you.

Of course I would like to thank my family for their endless support throughout my education, for believing in me at times when I did not, and for their never ending interest in something

they certainly do not understand. A special thanks to my mother who has supported me in so many ways and also gave me the possibility to rest during the summers at home and therefore be able to put all my energy into school and this thesis.

I would like to thank my friends in and outside of school, in Sweden and in the rest of the world, for listening to my fascination for optics, lasers and nonlinear technology and at many points telling me I am a geek and a nerd. Thank you for taking my mind of work, endless good times and so many dances, so much laughter and all those barbeques.

Finally, I would like to thank Prof. Fredrik Laurell for letting me work in the group and for spreading his knowledge, enthusiasm and for always having a laugh and a joke close to hand. It is an honor to work for and learn from you.

Table of Contents

1 Introduction

Background

Today it is common to use lasers, and hence electromagnetic radiation, for various kinds of medical applications, including surgery. Lasers at various wavelengths are used in many medical fields from cornea reshaping to cancer treatment and brain surgery [1,2,3]. Initial studies at free electron lasers (FEL) in the USA have shown that radiation at a wavelength of 6.45 μm is beneficial for surgical applications [4] since both water and proteins absorb radiation at that wavelength. FELs, however, are usually large facilities coupled to expensive accelerators which are not suitable to be integrated into a hospital.

This desired wavelength can be generated with quantum cascade lasers (QSL), but there are other demands on the radiation than the wavelength. To be suitable for surgery the radiation has to have rather high pulse energies in order to get efficient ablation of the cells while not damaging surrounding cells due to deposition of heat.

Generating the desired wavelength can be done with the use of nonlinear optical technology, optical parametric oscillators, and novel laser sources. These technologies make it possible to generate pulsed radiation at and close to the desired wavelength at high enough energies. The repetition rate of the pulsed radiation cannot be too high since that would result in a high average power and thermal damage to surrounding tissue, but has to be high enough to have efficient ablation. The pulse energy has be high enough to reach ablation threshold and the pulse length has to be long enough to not have too high peak intensities and short enough to have efficient non-linear conversion.

The objective of the work

The purpose of this thesis is to generate a beam with a wavelength of 3193.2 nm that has good coherence both spatially and temporally. This beam is later on supposed to seed another parametric process, hence the demands on a good beam quality. This can be achieved by using a pump beam of high quality and using a stable cavity. By having a good overlap between the TEM_{00} mode of the resonator and the pump beam waist a nice spatial coherence can in principle be obtained. The temporal coherence is in this case inherited from the pump beam. High quality pump beams requires lasers that operates in single longitudinal and transversal mode.

Lasers operating in multiple longitudinal and transversal modes are however attractive pump sources since they can be considered cheap, compared to lasers operating in single mode, while providing high energies. These lasers, however, are characterized by broad spectral bandwidth and large beam quality factors, M^2. In practical situations these beams are difficult to be focused to have a beam waist in the size of the fundamental mode of the resonator without substantial losses, even when working in the mid-infrared spectrum. This will make it difficult to generate a beam with high spatial coherence and also, the large bandwidth will be

transferred to the generated beams. Therefore other ways of generating highly coherent beams at the desired wavelengths are also investigated by using a multimode pump source.

A laser operating at multiple longitudinal and transversal modes can be converted into a conical beam, also called a Bessel beam, by using an axicon. These beams are attractive to be used as a pump sources for nonlinear processes since only the coherent part of the pump beam is exploited. Therefore, it is of interest to investigate how the coherence of a parametric device can be improved by the use of a conical pumping beam for nonlinear processes.

Outline of the thesis

The outline of this thesis is as follows:

In chapter 2 some theory of laser beams and resonators relevant for the thesis is described.

In chapter 3 the theory of nonlinear optical technology, optical parametric oscillators and various ways of phase matching is presented.

In chapter 4 the experiments performed throughout this work are described and analysed

Chapter 5 summarizes the work performed. Conclusions and discussion of the results and suggestions to further work are given.

2 Laser resonators and laser beams

Lasers are today common and important, both in research and in everyday life. They exist in everything from DVD-players to barcode scanners in the supermarket. In research they play a central role in a lot of areas; either as a “tool” or as research subject itself. The main topic of this thesis is not laser, but rather optical parametric oscillation (OPO) and optical parametric generation (OPG), which will be described in Chap. 3.3. Still, lasers are used as pump sources in all experiments in this thesis, and knowledge of laser beams and laser resonators is crucial for this work. Hence, a short description of the basic principles of lasers, laser beams and laser resonators follows.

A laser requires a resonator, an active medium (sometimes also called ‘gain’ or ‘laser’) and a source of energy. The energy source is generally called ‘pump’ and is used to create population inversion, i.e. excite the atoms to a higher energy level in the active medium. It is common to use flash lamps or lasers themselves as pump sources.

The resonator is built from mirrors and other optical elements e.g. beam splitters and polarizers. In the simplest case the resonator consists of two mirrors, where usually at least one is curved. One of the mirrors (in the case of a two mirror resonator) will have a reflectivity close to 100% for the laser wavelength, and it is usually called the input coupler. The other mirror will have a slightly lower reflectivity for the lasing wavelength and is called the output coupler.

The active medium in a laser can be a dye, gas, semiconductors, fluid or as all media used in this work, solid state materials, i.e. crystals.

The laser action will start when the active medium spontaneously emits a photon. That photon will be reflected by the mirrors in the resonator and eventually pass through the active medium again. By interacting with the medium, the photon will induce stimulated emission, creating more photons that are, ideally, a copy of the first photon. These will in turn start resonating as well and repeat the process over and over again, building up an electric field of high intensity in the resonator. Some of the photons will be coupled out of the resonator by the output coupler and create the laser beam. A sketch of a basic laser is shown in Fig. 2.1.

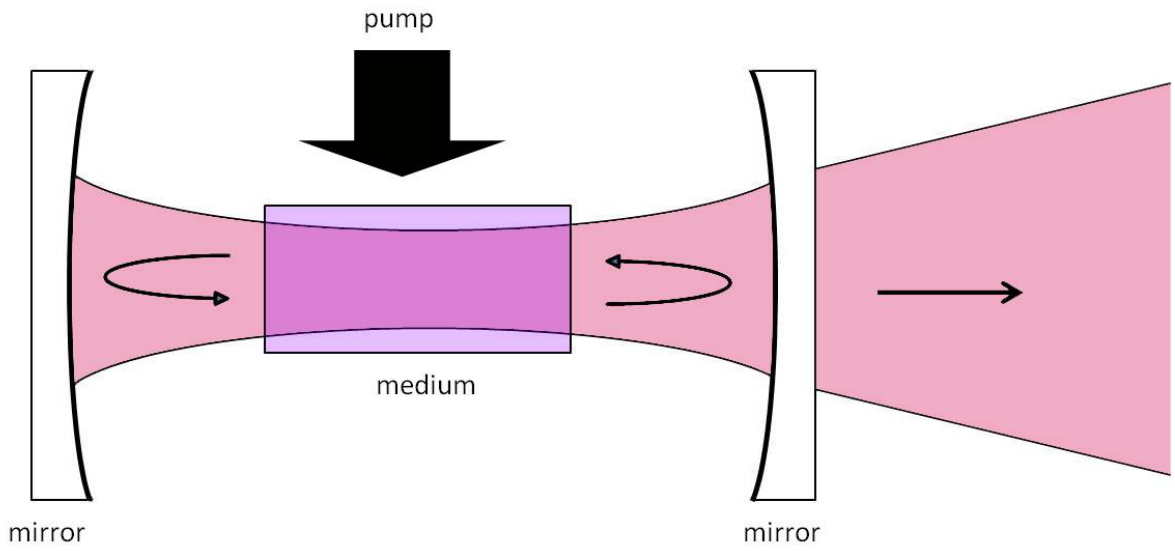

Figure 2.1: A schematic sketch of a laser, consisting of two mirrors an active medium and a pump source.

Lasers are attractive light sources since they are monochromatic and can propagate for a long distance and remain collimated. These features can be described more with the terms temporal and spatial coherence. Coherence is a property that is valid for all kinds of waves, not only light. Generally when talking about waves the term ‘wave front’ is introduced. A wave front can basically be described as an event, e.g. the wave has maximum amplitude, which occurs during every period as the wave propagates.

Temporal coherence describes how monochromatic a light wave is, the higher temporal coherence the more monochromatic the light wave is. The temporal coherence is usually given physically by a coherence length. This length describes for how long it is possible to predict how the wave fronts will propagate. If the wave front of the light is known at one point in time is it possible to predict how far the wave front has propagated at a later time. The only requirement is that the distance the wave has traveled during the time elapsed is shorter than the coherence length.

Spatial coherence is instead a measurement of how the light diverges as it propagates. Ideally the light would diverge as a perfectly spherical wave, emerging from a point source. For a highly spatially coherent wave is it possible to describe all points in space on a wave front by knowing only one point on the wave front.

2.1 Gaussian beams

The light in a laser will, as previously stated, propagate within a resonator, and only parts of it will be coupled out and create the laser beam. This propagation within the resonator will impose conditions on how the light can propagate, both in longitudinal and transversal direction. The limitation on how the beam can propagate will determine the beams transversal

intensity distribution. What is called a Gaussian beam can build up within the resonator constructed of curved mirrors [5]. It is called a Gaussian beam due to the intensity profile of the electric field that is built up in the transversal direction. When coupled out of the resonator the light will keep its Gaussian intensity distribution. Other kinds of resonators will have other transversal intensity distributions, which sometimes are rather close to Gaussian. However Gaussian beams possess physical properties which are of interest when working with lasers, as will be shown later on in this chapter.

The Gaussian beam is an eigensolution to the paraxial wave equation [5], or in a more physical description, it is the only way the light wave can build up in free space and reproduce itself during every round trip when being limited by mirrors as in a resonator. The electric field for the Gaussian beam propagating along the z-axis is given by

$$E(r,z) = E_0 \frac{\omega_0}{\omega(z)} e^{-i(kz-\varphi(z))} e^{-i\left(\frac{kr^2}{2q(z)}\right)}. \quad \textbf{(2.1)}$$

Here $\omega(z)$ is the spot size of the beam, ω_0 is the spot size at the beam waist and $q(z)$ is the complex beam parameter given by

$$\frac{1}{q} = \frac{1}{R} - i\frac{\lambda}{\pi n \omega^2}, \quad \textbf{(2.2)}$$

where R is the radius of curvature of the wave fronts, n is the refractive index of the medium the wave is traveling in and ω the spot size of the beam. The real part of this equation resembles the description of a spherical wave front. That is because curvatures of the wave fronts of a Gaussian beam are very close to ideally spherical when propagating.

There are higher order solutions to the paraxial wave Equation as well and they are due to symmetry reasons a product of Hermite polynomials with a Gaussian function

$$E_{n,m} = E_0 H_m\left(\sqrt{2}\frac{x}{\omega}\right) H_n\left(\sqrt{2}\frac{y}{\omega}\right) e^{-\frac{x^2+y^2}{\omega^2}}. \quad \textbf{(2.3)}$$

Here m and n describes the higher order in the horizontal and vertical direction. The notation TEM_{mn} is used as notation for the various eigenmodes. The lowest order modes for m,n=0,1,2,3 are displayed in Fig. 2.2. All of these solutions are called *transversal modes* of the laser.

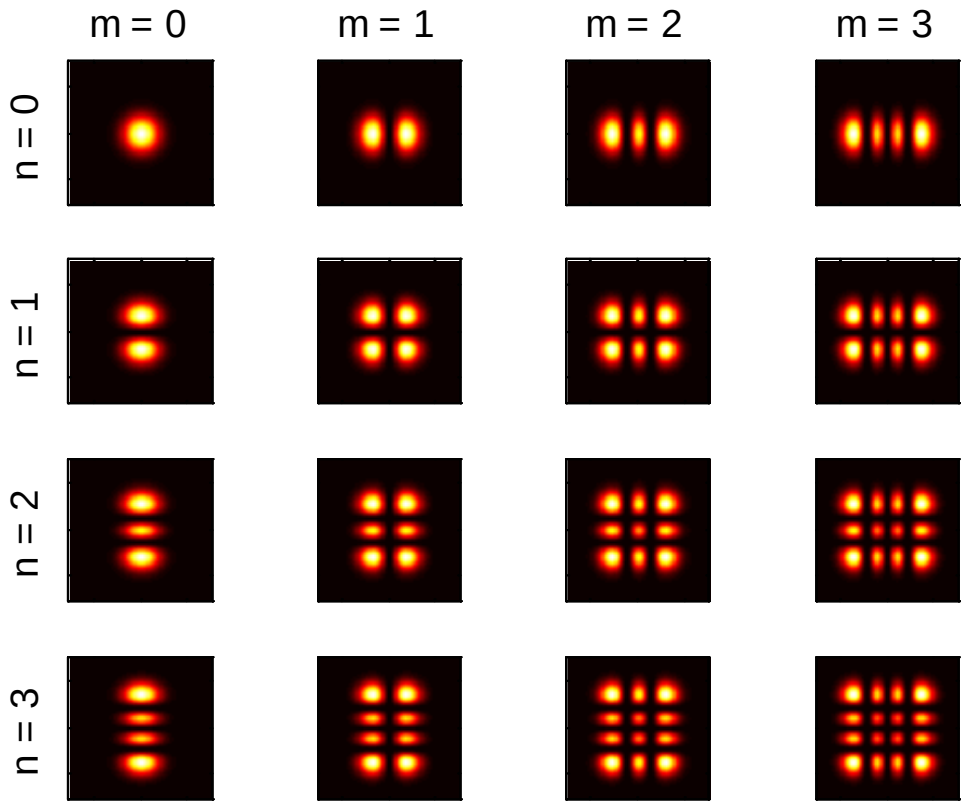

Figure 2.2: Transversal Gaussian mode patterns for m,n=0,1,2,3.

Although the Gaussian distribution extends to infinity it is convenient to define a beam radius. The beam radius of a Gaussian beam is generally defined as the value where the intensity is reduced by a factor of $1/e^2$ in respect to the peak intensity. The minimum radius of the beam is called the spot size and the beam radius can then be described by

$$\omega(z) = \omega_0 \left[1 + \left(\frac{\lambda z}{\pi \omega^2}\right)^2\right]^{\frac{1}{2}}. \qquad \textbf{(2.4)}$$

An important parameter of Gaussian beams is the *Rayleigh range*. The Rayleigh range is the depth of focus of the Gaussian beam and the wave fronts can be approximated with plane waves within the Rayleigh range. One defines the Rayleigh range as the distance from the beam waist to where the beam area has doubled, i.e. where the beam radius has increased by a factor of $\sqrt{2}$. It follows from Eq.(2.4) that it can be written as

$$z_R = \frac{\pi \omega^2}{\lambda}. \qquad \textbf{(2.5)}$$

Since it is possible to focus a Gaussian beam down to the diffraction limit, they are said to be diffraction limited.

In reality laser beams are seldom perfectly Gaussian. Instead, they are usually superpositions of the lowest order mode and higher order modes and the beam radius can then be described by the adjusted function

$$W(z) = W_0 \left[1 + \left(M^2 \frac{\lambda z}{W_0 \pi}\right)^2\right]^{\frac{1}{2}}, \quad \textbf{(2.6)}$$

where M^2 is called the *beam quality factor*. It measures how close to a perfect Gaussian beam the laser beam is, and a good measure of the spatial coherence of the beam, since a perfect Gaussian beam is highly spatially coherent.

A convenient way on measuring the beam radius of an arbitrary beam is to use the knife-edge technique [6,7]. A razor blade is used to cut the beam perpendicular to the direction of propagation. The position of the razor blade is recorded at the positions where the intensity is 16% and 84% of the total intensity. The distance between those positions of the razor blade is the beam radius. By measuring the beam radius at several points along the optical axis of a focused laser beam and then fitting the data to Eq.(2.6) the M^2 of an arbitrary beam can be determined. However, this method is only valid for beams that are close to Gaussian beams, that is, with a not too high M^2.

2.2 Stable Resonators

As previously stated a resonator, also called a cavity, is a requirement for a laser to operate. It is also used in some nonlinear processes in order to enhance gain and amplification [5]. The resonator also has an impact on the beam quality factor of the generated beam.

It is common to have standing waves in the resonator although traveling wave cavities exist. After one round trip in the cavity is it desirable for the light to have a phase shift of 2π in order to have constructive interference and for the light of a certain wavelength to find resonance. That will impose a condition on which wavelengths, or frequencies, that will be able to resonate, i.e to impose a standing wave inside the cavity. These are given by

$$m\lambda = 2L. \quad \textbf{(2.7)}$$

Here L is the optical path length of the cavity, λ is the wavelength and m is an integer number. m is usually large, in the order of 10^5, since the cavity is often much longer than the wavelength.

From Eq.(2.7) is it easy to calculate the frequency spacing between two longitudinal modes. The result shows that the mode separation is dependent on the length of the resonator. The frequency spacing between two modes is

$$\Delta\upsilon = \frac{c}{2L}. \quad \textbf{(2.8)}$$

A resonator generally consists of basic optical elements like mirrors, lenses and eventually other more complex components. Among them are beam splitters, volume Bragg gratings, Pockels cells and other elements that imposes various properties to the generated beam.

These elements can in theory be described by a 2x2 matrix, in what is called the ABCD-formalism [5].The ABCD formalism is used for ray tracing in optical systems and the matrices describes mathematically how the distance, r, and the angle , θ, to the optical axis are affected by a given optical element by

$$\begin{bmatrix} r_2 \\ \theta_2 \end{bmatrix} = \begin{bmatrix} AB \\ CD \end{bmatrix} \begin{bmatrix} r_1 \\ \theta_1 \end{bmatrix}. \quad \textbf{(2.9)}$$

An important property of these matrices is that they are unimodular, that is, AD-BC=1. From this follows that a product of several matrices will be unimodular as well.

This formalism can be combined with the theory of Gaussian beams by

$$q_2 = \frac{Aq_1 + B}{Cq_1 + D}. \quad \textbf{(2.10)}$$

The complex beam parameter is given by Eq(2.2).

By multiplying the matrices of all the elements in the cavity for one round trip in the cavity a matrix for the entire system can be calculated. Combined with the requirement that the beam should regain its shape after one roundtrip, in order for the resonator to be considered stable, the following relation is obtained

$$q = \frac{Aq + B}{Cq + D}. \quad \textbf{(2.11)}$$

Because of the unimodular property of the ABCD is it then possible to write the complex beam parameter, q, as

$$\frac{1}{q} = \frac{D - A}{2B} \pm i\frac{\sqrt{1 - \left(\frac{D+A}{2}\right)^2}}{B}. \quad \textbf{(2.12)}$$

Comparing this expression to Eq.(2.2), which relates the complex beam parameter, q, to the beam radius and the radius of curvature of the beam, makes it possible to formulate a condition for when the resonator is stable. Since the ω_0^2 must be a real and positive, the relation in the square root in Eq.(2.12) must be positive as well, that is

$$\left|\frac{D + A}{2}\right| \leq 1. \quad \textbf{(2.13)}$$

This relation is known as the stability condition for a resonator. It also shows how sensitive the cavity is to misalignment of the components, depending on the value of the stability condition.

Since q is related to the radius of curvature, R, and the beam radius, ω, is it possible to relate these entities to the ABCD-matrix for the system. At the chosen plane of reference, where the round trip in the cavity starts and ends, is it possible to relate the beam radius and the radius of curvature as

$$\omega = \left(\frac{\lambda}{\pi n}\right)^{\frac{1}{2}} \frac{|B|^{\frac{1}{2}}}{\left[1-\left(\frac{D+A}{2}\right)^2\right]^{\frac{1}{4}}}. \qquad \textbf{(2.14)}$$

Eq.(2.14) together with Eq.(2.11) makes it possible to trace the beam radius throughout the resonator. This is valid for any resonator, not only two mirror resonators. It is possible to simulate the evolution of the beam inside the cavity by using numerical calculations (the program used in this work is named Winlase).

This formalism makes it possible to predict how the beam will look in the resonator but also how it will behave when coupled out of the resonator. In order for the beam that is created in the resonator to have the lowest order mode is it necessary for the active medium to be pumped in an area that has the same size, or smaller, than the area that is created by the mode supported by the resonator, too. If a bigger area is utilized in the active media higher order transversal modes be will supported. Higher order transversal modes can also be an effect of a misaligned cavity, and can be removed by proper alignment.

2.3 Bessel beams

Bessel beams are usually said to be free from diffraction [8], which is not entirely true. Bessel beams diffract, as all light does, but they diffract in such a way that their transversal shape remains unchanged. This is very convenient when the beam encounters a small obstacle since it will regain its original shape afterwards.

A Bessel beam is a coherent beam with a transverse intensity distribution of a Bessel function. The electric field of these beams can be described by [9]

$$E(\rho, \phi, z) = E_0 e^{-i(k_z z-\omega t)} \cdot e^{\pm in\phi} \cdot J_n(k_\rho \rho), \qquad \textbf{(2.15)}$$

where $k_z^2+k_\rho^2=k^2$, k being the wave vector. The radial, azimuthal and longitudinal coordinates are ρ, ϕ and z, and n is the integer which indicated the order of the Bessel function, J_n. Higher order Bessel beams can be generated and will then have a central minimum instead of having a central maximum. In this work a zeroth order beam is used since the confined central peak is of interest for pumping the nonlinear process.

A more physically intuitive description of a Bessel beam is to describe it a plane wave that are caused to interfere with itself, by propagating in a cone. The light is refracted towards the optical axis, and forming a cone and will ultimately interferes with itself, causing a transverse intensity pattern of a Bessel function. From this description is it intuitive to understand why these beams can be considered diffraction free. Every point along the focal line is created

when different parts of the beam interfere. Therefore, if the beam encounters a small obstacle, it will regain its transverse shape after the obstacle.

2.3.1 Axicons

One way to generate laser beams with a transverse intensity distribution of a Bessel function is to use an axicon. An axicon is a lenslike element which instead of creating a point focus, creates a focal line along the optical axis. There are different kinds of axicons, such as refractive, diffractive and reflective axicons [10]. In this work a refractive axicon is used. The axicon has a shape of a cone, as can be seen in Fig. 2.3. The first refractive axicon was suggested in 1954 by McLeod [11].

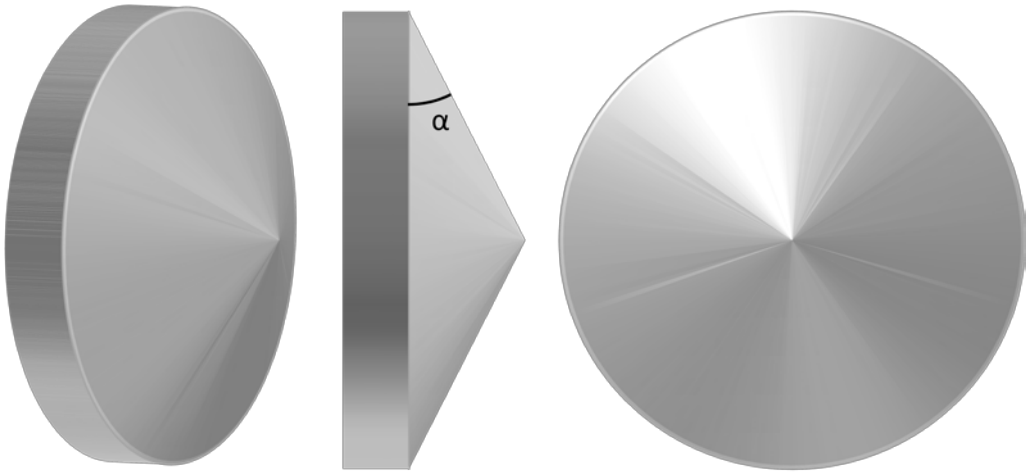

Figure 2.3: Sketch of an axicon. The axicon is defined by its top angle, or more commonly, the angle α

The axicon will introduce a phase shift in the beam and cause it to refract towards the optical axis and interfere with itself, and by that create a transverse intensity profile of a Bessel function, and longitudinally create what can be called a focal line. The phase shift that is introduced is related to the prism angle, α, (Fig. 2.3). The phase shift introduced by an axicon with refractive index n on an incoming beam of light is

$$\varphi(\rho) = (n - 1)\rho \cos \alpha. \tag{2.16}$$

Generating a perfect Bessel beam with an infinitely long focal line is impossible. It would require an axicon, as well as an incident beam, of infinite extent, which is highly unphysical. The finite extent of the axicon and the incident beam will cause a finite extent of the Bessel distribution and a finite extent of the focal line. This can be understood from Fig. 2.4.

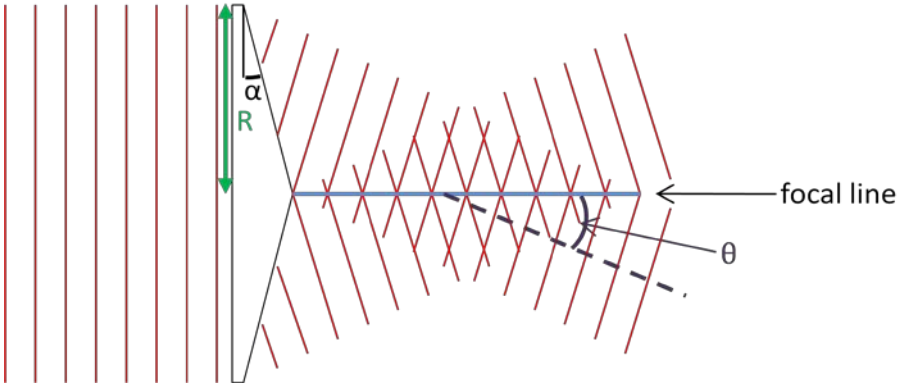

Figure 2.4: Illustration of how the axicon refracts a beam consisting of planar wave fronts, creating a focal line.

From Fig.2.4 the finite extent of the focal line, z_{max}, can be approximated. The length of the focal line can be related to the angle at with which the axicon refracts the light, θ, and the radius of the incident beam, R, as

$$z_{max} = \frac{R}{\tan(\theta)}. \tag{2.17}$$

The angle θ can be related to the top angle of the axicon by

$$\theta = (n-1)\alpha, \tag{2.18}$$

The radial part of the wave vector, k_ρ can hence be written

$$k_\rho = k\frac{\tan(\theta)}{\sqrt{1+\tan^2(\theta)}}. \tag{2.19}$$

The $1/e^2$ radius of the central maximum can be approximated for a zeroth order beam and can be calculated as

$$\omega_0 = \frac{1.3258}{k_\rho}, \tag{2.20}$$

where 1.3258 is the argument for when a zeroth order Bessel function intensity is reduced by $1/e^2$ and k_ρ is the radial component of the wave vector for the refracted beam.

Both the extent and the radius of the central maximum are related to which angle, θ, the beam is refracted towards the optical axis. A long extent of the focal line requires a small angle of refraction, which a small central maximum requires a large angle of refraction. It is therefore a tradeoff between a long extent of the focal line and a focus with small radius. And for every application this tradeoff needs to be considered.

In order to calculate the electric field and the intensity after the axicon, scalar diffraction theory can be used [12]. There are several integrals, based on the Fresnel-Kirchhoff diffraction theory [13], which can be used for calculating the electric field at any point in space after a diffracting aperture. They, however, require knowledge about the electric field at the diffracting aperture. The Rayleigh-Sommerfeld integral, Eq.(2.21), is convenient to use

since it only requires knowledge of the electric field at the aperture, but not of the space derivative of the electric field at the aperture.

$$E(P_0) = -\frac{k}{2\pi}\int_{aperture} \mathrm{E_0 e^{-i(k_z z-\omega t)}} \cdot \mathrm{e^{\pm in\phi}} \cdot \mathrm{J_n(k_\rho \rho)} \cdot \frac{\exp(ikr_{01})}{r_{01}} \cdot \left(i - \frac{1}{kr_{01}}\right) \cdot \cos(\Theta)\, ds, \tag{2.21}$$

$$r_{01} = \sqrt{\left(x_{aperture} - x_{obs}\right)^2 + y_{obs}^2 + z^2},$$

$$\cos(\Theta) = \frac{z}{r_{01}}.$$

Here r_{01} is the distance between a point in the aperture and the point, P_0.

By evaluating the Rayleigh-Sommerfeld integral the intensity after the axicon can be evaluated, as shown in Figs. 2.5.

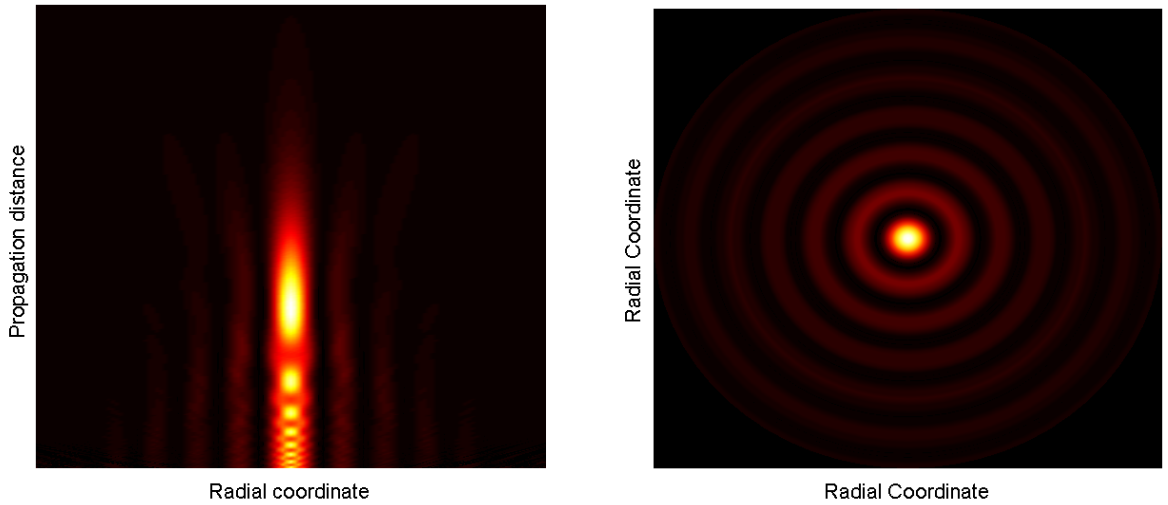

(a) (b)

Figure 2.5: Simulation of a Bessel beam assuming incoming plane waves with a wavelength of 1064 nm and an aperture size of 1 cm. **a)** Longitudinal intensity distribution. **b)** Radial intensity distribution.

As the beam propagates beyond the extent of the focal line it will diffract into a ring. This can be shown from an evaluation of Eq.(2.21) at a position further away than the calculated extent of the focal line. The beam will diffract into a ring in the far field with radius and thickness related to the prism angle, α, of the axicon. This can be used when aligning the axicon as seen in Figs. 2.6.

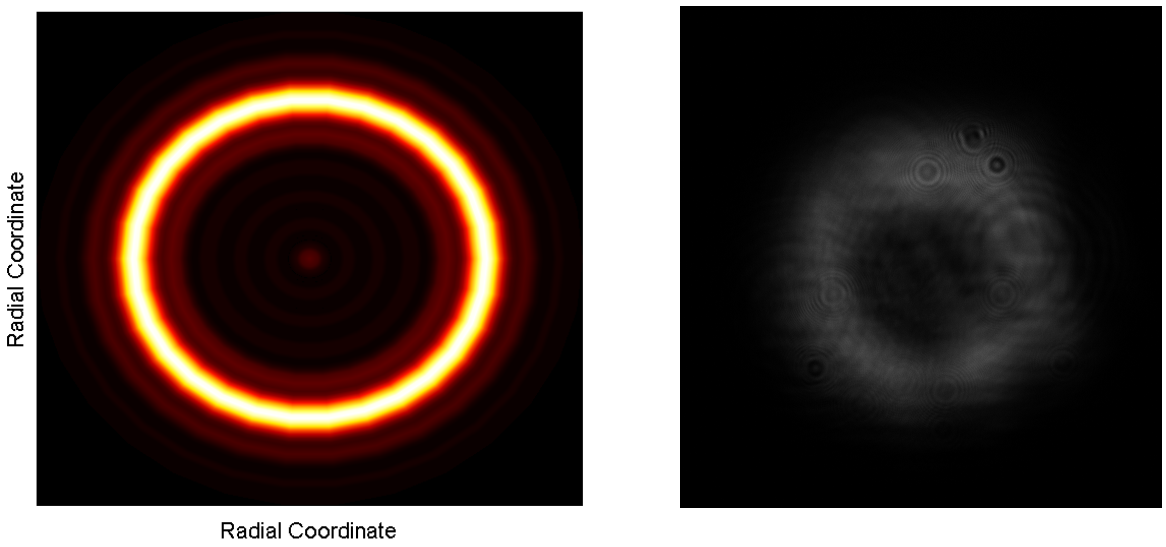

(a) (b)

Figure 2.6: Far field diffraction pattern of a Bessel beam **(a)** simulated with same conditions as Figs. 2.5 and **(b)** recorded with a CCD camera from the actual setups in Chap 4.2.

The simulations shown above are done assuming a perfectly coherent beam. When using a partially coherent beam the transversal Bessel distribution will be distorted and the visibility of the interference pattern will decrease [8], that is, energy will be located also in the minima of the interference pattern. For a partially coherent beam operating in multiple transversal modes, a coherence radius can be introduced. This is the radius of the beam for which the beam can interfere with itself due to its partial coherence. The extent of the focal line can then be calculated by using the coherence radius instead of the beam radius in Eq.(2.17).

3 Nonlinear Optics

Nonlinear optics is the field of optics that describes the phenomena arising when light is interacting in a nonlinear manner with matter. Nonlinear optics makes it possible to generate wavelengths that are usually not usually available or difficult to reach with regular lasers by exploiting nonlinear interactions. Moreover it also describes how it is possible to create ultra short laser pulses and laser pulses with very high energy and optical-to-optical processing signals. The first demonstration of nonlinear optics was done in 1961 [14], only a one year after the first laser was demonstrated [15].

Generation of new wavelengths not available from regular lasers through nonlinear optics is convenient and rather efficient. For the process of wavelength conversion to take place a material with a nonlinear polarization, induced by an applied electric field, is required. The polarization of materials that can be described by [16]

$$P = \varepsilon_0 \sum_{n=1}^{\infty} \chi^{(n)} \cdot E^n. \tag{3.1}$$

Here $\chi^{(n)}$ is the n^{th} order susceptibility of the material induced by the electric field E propagating into the material. $\chi^{(n)}$ is a tensor of rank n+1. The first order term $\chi^{(1)}$ accounts for the refractive index(real part) and the linear absorption(imaginary part) of the material. The second order term, $\chi^{(2)}$ describes tree-wave mixing processes and is responsible for nonlinear processes, like second harmonic generation (SHG), optical parametric generation (OPG) and optical parametric oscillation (OPO). This component of the susceptibility only exists for materials with a lack of inversion symmetry, most commonly the non-centrosymmetric crystals. Of interest is also the third order term $\chi^{(3)}$, which is responsible for third order nonlinear effects and it exists in all materials, also the symmetric ones, at high enough intensities of the stimulating electric field, E. Higher order terms are generally not of interest since they are too small. For this work only the second order processes are of interest. It means the term to take into account in Eq.(3.1) is then

$$P_i^{(2)} = \varepsilon_0 \sum_{jk} \chi_{ijk}^2 \cdot E_j \cdot E_k, \tag{3.2}$$

where i,j,k are the three different directions of polarization.

In experimental results it is common to express $\chi^{(2)}$ as a new susceptibility tensor *d* by

$$d_{ijk} = \frac{1}{2}\chi_{ijk}. \tag{3.3}$$

Because of symmetry reasons is it possible to compress the components down to the following matrix [17]

$$d_{ij} = \begin{vmatrix} d_{11} & d_{12} & d_{13} & d_{14} & d_{15} & d_{16} \\ d_{21} & d_{22} & d_{23} & d_{24} & d_{25} & d_{26} \\ d_{31} & d_{32} & d_{33} & d_{34} & d_{35} & d_{36} \end{vmatrix}. \quad \textbf{(3.4)}$$

For $KTiOPO_4$, KTP, which is used in this work, this matrix is [18]

$$d_{ij} = \begin{vmatrix} 0 & 0 & 0 & 0 & d_{31} & 0 \\ 0 & 0 & 0 & d_{32} & 0 & 0 \\ d_{31} & d_{32} & d_{33} & 0 & 0 & 0 \end{vmatrix}. \quad \textbf{(3.5)}$$

The values of these coefficients can be found in [19]

When working with narrow bandwidths, as in lasers, is it convenient to work in the Fourier domain. This will make it possible to describe the induced polarization in the material as

$$P_i^{(2)}(\omega_\alpha) = \varepsilon_0 \sum_{jk} \sum_{\beta\gamma} \chi_{ijk}^2(-\omega_\alpha; \omega_\beta \omega_\gamma) \cdot E_j(\omega_\beta) \cdot E_k(\omega_\gamma). \quad \textbf{(3.6)}$$

Here ω_α is the generated angular frequency from the electric fields with angular frequencies ω_β and ω_γ.

Nonlinear interactions in a medium must respect the conservation of energy and momentum. The conservation of energy describes how the energy of a photon will be transferred into other photons in the nonlinear process. The condition of energy conservation is given by

$$h\omega_1 = h\omega_2 + h\omega_3, \quad \textbf{(3.7)}$$

where the interacting electric fields has the angular frequencies ω_1, ω_2 and ω_3.

In the case of second order processes the following are the most common ones:

Second Harmonic Generation (SHG):	$\omega_1 + \omega_1 = \omega_2$
Sum Frequency Generation (SFG):	$\omega_1 + \omega_2 = \omega_3$
Difference Frequency Generation (DFG):	$\omega_1 - \omega_2 = \omega_3$
Optical Parametric Generation (OPG):	$\omega_1 = \omega_2 + \omega_3$
Optical Parametric Amplification (OPA):	$\omega_1 = \omega_2 + \omega_3$
Optical Parametric Oscillation (OPO):	$\omega_1 = \omega_2 + \omega_3$

When working with OPG, OPO, and OPA one usually denotes the first frequency, which is the frequency providing the parametric process with energy, as the pump frequency, ω_p. The generated frequencies are called signal, ω_s, and idler, ω_i, where the lower frequency (and

hence longer wavelength) is called the idler. Over all is the relation $\omega_p \geq \omega_s \geq \omega_i$ valid for all parametric processes.

It can be observed that the same energy transfer is involved in DFG, OPG, OPA and OPO. What mainly differs in the parametric processes is the amount of energy that is transferred between the different frequencies involved. For DFG the energies of the pump and signal of the same order are of magnitude. In OPG the process is provided by energy only from the pump beam and both the signal and the idler are generated in the process. The OPA is provided with energy from the pump but also seeded with a weaker beam of the signal frequency in order to promote the desired frequencies. OPO is OPG (or sometimes OPA) where a resonator, which is resonating for the signal or idler, or sometimes both, is used to increase the efficiency of the energy conversion.

From the theory of nonlinear optics the energy transfer between the different frequencies can be calculated from the wave equation combined with Maxwell's equations and the nonlinear polarization of the material [16] as

$$\nabla^2 E_z(\omega_n) + k_n E_z(\omega_n) = -\frac{\omega_n}{c^2} P_z^{nl}(\omega_n), \tag{3.8}$$

where is E_z is the electric field in chosen direction (z-direction) with an angular frequency ω_n and a wavevector k_n, and p_z^{nl} is the the nonlinear polarization of the material in which the electric field is propagating. Here n is an interger which has the value of the number of interacting frequencies.

Using the slowly varying envelope approximation, SVEA, and evaluating Eq.(3.8) and collecting terms depending on the different frequencies will give the following equations for the energy transfer

$$\begin{aligned}
\frac{dE(\omega_1)}{dz} &= -i\frac{\omega_1 d_{eff}}{cn_1} E(\omega_3) E(\omega_2) e^{i\Delta kz}, \\
\frac{dE(\omega_2)}{dz} &= -i\frac{\omega_2 d_{eff}}{cn_2} E(\omega_1) E^*(\omega_3) e^{-i\Delta kz}, \\
\frac{dE(\omega_3)}{dz} &= -i\frac{\omega_3 d_{eff}}{cn_3} E(\omega_1) E^*(\omega_2) e^{-i\Delta kz}.
\end{aligned} \tag{3.9}$$

3.1 Phase matching

From Eq.(3.9) the coefficient Δk can be observed in all of the three equations. Δk is the difference in momentum, or wave vectors, between the different waves and can be written

$$\Delta k = k_1 - (k_2 + k_3). \tag{3.10}$$

This can be considered the phase mismatch in the process, where k is the wave vector of a light wave. In the case of perfect phase matching, that is when $\Delta k=0$, all the momentum of the

pumping photons will be transferred to the photons created in the process. This is, however, seldom the case. Since all materials are dispersive, the interacting waves will have different phase velocities and hence get out of phase after propagating for some distance, called the coherence length, in the medium. This can be seen from looking at the wave vector which is dependent on the refractive index, $k_i=2\pi n_i/\lambda_i$. These usually have different value for all wavelengths propagating in the same material. A result of this phase mismatch is back conversion, where the desired waves are converted back to the original wave until the waves get in phase with each other again, after another coherence length. Full phase matching is desired in order to have a highly efficient of the process, but it is hard to achieve.

One common way of achieving phase matching is Birefringent Phase Matching, BPM. Here the nonlinear crystal is oriented so that the ordinary refractive index of one wavelength matches the extraordinary index of refraction for the other generated wavelength. When several wavelengths are involved, such as in a nonlinear process, this is hard to achieve. Also, walk off, where one of the beams changes direction of propagation in the crystal, and distortion of the beam profile of the generated beam, are effects that occur in BPM as well. Another negative aspect of this kind of phase matching is that it does not permit to exploit the highest nonlinear coefficients, which will lower the efficiency of the process.

The phase matching technique employed this work is called Quasi Phase Matching, QPM. Quasi phase matching was first suggested in 1962 [20]. By using ferroelectric crystals and inverting the intrinsic polarization every time the original beam and the generated beams get out of phase by π, the phase matching can be periodically achieved to have gain throughout the entire crystal.

QPM also makes it possible to use the largest nonlinear coefficient of the crystal. Since the group phase velocity is controlled by the domain grating the crystal can be orientated in such a way that the largest nonlinear coefficients are used. This will further increase the efficiencies of the nonlinear process.

In this work the switching of the polarization is done by applying an electric field, higher than the coercive field, and by that periodically reverting the polarization of the crystal with a certain period. If this switching of the intrinsic polarization is done properly it is possible to let the interacting waves propagate in phase throughout the entire length of the crystal, and therefore get a gain of the nonlinear process and avoid destructive interference and back conversion. This can be described as adding a wave vector to Eq.(3.10) with the size

$$k_{QPM} = \frac{2\pi m}{\Lambda}, \tag{3.11}$$

where Λ is the period of the domain grating, and m is the order of the spatial harmonic. For first order phase matching the highest efficiency is obtained for a duty cycle of 50%. It is therefore desirable to have a duty cycle of 50%, meaning the intrinsic polarization is switched every time the pump beam and generated beams get π out of phase.

The effective nonlinear coefficient, with a duty cycle of 50%, is then given by

$$d_{eff} = \frac{2}{m\pi} d_{ij}. \quad \textbf{(3.12)}$$

Eq.(3.10) then becomes

$$\Delta k = k_3 - (k_1 + k_2) + k_{QPM}. \quad \textbf{(3.13)}$$

For perfect phase matching it is desirable to have Δk=0, which will then give an expression for the desired size of the wave vector introduced by the domain grating

$$k_{QPM} = k_3 - k_1 - k_2. \quad \textbf{(3.14)}$$

From Eq.(3.12) and Eq.(3.14) can then the desired grating period for first order QPM (m=1) be calculated as

$$\Lambda = \frac{2\pi}{k_3 - k_1 - k_2}. \quad \textbf{(3.15)}$$

The technique of creating the domain grating when obtained by periodically applying a strong electric field is it called periodic poling and is usually abbreviated PP in front of the crystal name, i.e. PPKTP for the crystals used in this work.

3.2 Phase matching with Bessel beams

The derivation in the previous section is done for plane waves, with all waves propagating in the same direction. That is not the case when working with beams having a transverse intensity distribution of a Bessel function. These beams are considered to be conical beams, with their wave vectors forming a cone. The derivation of the phase matching conditions must therefore be changed to consider the direction of the interacting beams. The interacting beams will now propagate in different directions. This is illustrated in Fig. 3.1.

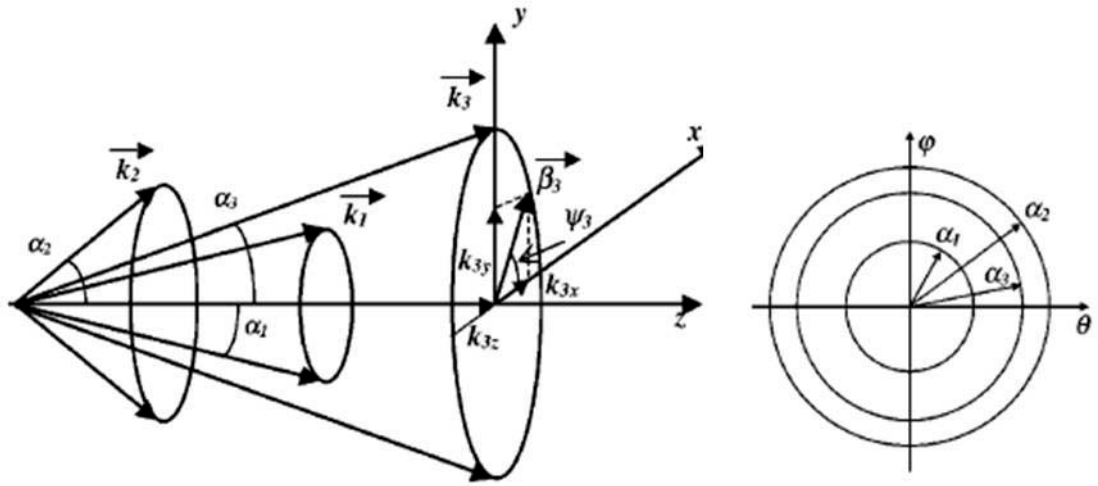

Figure 3.1: Illustration of the phase matching with conical beams in the longitudinal and transversal plane [21].

The interacting waves have to be phase matched, not only in the longitudinal direction but also transversally. The derivation of the phase matching with conical beams has been made by Piskarskas et al. [21,22], Pasiskevicius [23] and Tewari [24] and will not be performed in detail here.

Since the interacting waves are no longer propagating in the same direction, it is important to do not only take into account the longitudinal direction of the phases, but also the transversal direction. The phase matching conditions for an OPO in the three Cartesian coordinates can be written

$$\begin{aligned} k_{sx} + k_{ix} &= k_{px}, \\ k_{sy} + k_{iy} &= k_{py}, \\ k_{sz} + k_{iz} &= k_{pz}. \end{aligned} \tag{3.16}$$

Here *k* is the wavevector, the subscripts *x*,*y* and *z* denotes the Cartesian space coordinates with the optical axis (i.e. the direction of propagation) along the z-axis, and subscripts *s*,*i* and *p* denotes the signal, idler and pump waves respectively.

When using a crystal which is periodically poled the QPM period of the ferroelectric grating must be accounted for. The grating period will introduce and extra wave vector into Eq.(3.16) and the phase matching condition will now be

$$\begin{aligned} k_{sx} + k_{ix} &= k_{px}, \\ k_{sy} + k_{iy} &= k_{py}, \\ k_{sz} + k_{iz} + k_{QPM} &= k_{pz}. \end{aligned} \tag{3.17}$$

The first two expressions in Eq.(3.17) account for the transverse phase matching. It is the coupling, and hence the phase matching, between the interacting waves in the transverse plane that determines the parametric gain of the process. As Piskarskas et al. have shown in [21] only certain combinations of the azimuthal angles result in a high parametric gain. The maximum parametric gain is obtained when the following conditions are fulfilled:

$$\begin{aligned} &(i)\psi_s = \psi_i = \psi_p, \\ &(ii)\psi_s = \psi_p, \;\; \psi_i = \psi_p + \pi, \\ &(iii)\psi_i = \psi_p, \;\; \psi_s = \psi_p + \pi, \end{aligned} \tag{3.18}$$

where ψ is the angle from the x-axis in the transversal xy-plane as seen in Fig. 3.1.

The first condition is collinear phase matching, with all beams propagating in the same direction. That would however result in both signal and idler being divergent, propagating in a cone, which is not desired here. Conditions (ii) and (iii) are noncollinear phase matching, which makes it possible to create beams propagating in different directions. This makes it possible to generate a signal (or idler) that will propagate along the optical axis, and create a highly coherent beam. Using condition (ii) in the momentum conservation Eq.(3.17) becomes

$$k_s \cos\alpha_s + k_i \cos\alpha_i + k_{QPM} = k_p \cos\alpha_p\,,$$
$$k_s \sin\alpha_s - k_i \sin\alpha_i = k_p \sin\alpha_p, \quad \textbf{(3.19)}$$

and condition (iii) in will result in Eq.(3.17).

$$k_i \cos\alpha_i + k_s \cos\alpha_s + k_{QPM} = k_p \cos\alpha_p\,,$$
$$k_i \sin\alpha_i - k_s \sin\alpha_s = k_p \sin\alpha_p. \quad \textbf{(3.20)}$$

Evaluating Eq.(3.19) and Eq.(3.20) will show that two independent signal-idler pairs can be created simultaneously for each domain grating period of the crystal. The ferroelectric grating period can be calculated by setting α_s=0 and α_i=0 respectively. The choice of the resonator and the reflectivity of the resonator mirrors, can be used to control which signal-idler pair that will be dominant in the OPO.

3.3 Optical parametric oscillation

As described in previous sections, optical parametric oscillation (OPO) is a nonlinear process that transfers energy of one wavelength into two longer wavelengths. The OPO consists of a resonator, that will help to control the process, and a nonlinear crystal. In this work PPKTP with a proper QPM period designed to obtain the desired wavelengths, has been used.

There are two different kinds of OPOs. There is the singly resonant OPO where only the signal (or the idler) is resonating in the cavity. The other type is the doubly resonant OPO where the cavity is resonant for both the signal and the idler. This requires the cavity to be very stable since two waves that are coupled to each other must be resonant at simultaneously. A slight shift in cavity length, by for instance thermal drift, will shift the resonant frequencies, making the cavity difficult to keep stable. The OPOs built in this work were singly resonant for the signal wave.

There are similarities between an OPO and a laser. Both are processes where a wave is resonating within a cavity with an active medium. In an OPO, however, the nonlinear response is very fast (a few fs), compared to the cavity roundtrip time, and no energy is stored within the crystal. Whilst energy is absorbed in the active laser material and the phase of the pumping wave is forgotten when the stimulated photon is emitted, the phase of the pumping wave is remembered in the signal and idler waves. The parametric process also has a threshold of operation and can show a longitudinal mode structure, just like the laser.

To get the parametric process started high intensities are required and therefore the risk of damaging the crystals and optical components need to be considered. Measurements by Yoshida et al. [25] and Hildenbrand et al. [26] have shown KTP has a damage threshold of approximately 20 J/cm^2 for light with a wavelength of 1 μm and nanosecond pulses. There are, however, risks of damaging other optical components, especially the dielectric coating on the mirror used, too.

From Eq.(3.9) it can be seen that the coupled wave equations for an OPO are

$$\begin{aligned}\frac{\mathrm{dE}(\omega_\mathrm{p})}{\mathrm{dz}} &= -\mathrm{i}\frac{\omega_\mathrm{p}\mathrm{d}_\mathrm{eff}}{\mathrm{cn}_\mathrm{p}}\mathrm{E}(\omega_\mathrm{i})\mathrm{E}(\omega_\mathrm{s})\mathrm{e}^{\mathrm{i}\Delta\mathrm{kz}},\\ \frac{\mathrm{dE}(\omega_\mathrm{s})}{\mathrm{dz}} &= -\mathrm{i}\frac{\omega_\mathrm{s}\mathrm{d}_\mathrm{eff}}{\mathrm{cn}_\mathrm{s}}\mathrm{E}(\omega_\mathrm{p})\mathrm{E}^*(\omega_\mathrm{i})\mathrm{e}^{-\mathrm{i}\Delta\mathrm{kz}},\\ \frac{\mathrm{dE}(\omega_\mathrm{i})}{\mathrm{dz}} &= -\mathrm{i}\frac{\omega_\mathrm{i}\mathrm{d}_\mathrm{eff}}{\mathrm{cn}_\mathrm{i}}\mathrm{E}(\omega_\mathrm{p})\mathrm{E}^*(\omega_\mathrm{s})\mathrm{e}^{-\mathrm{i}\Delta\mathrm{kz}}.\end{aligned} \tag{3.21}$$

From these equations it can be seen that the energy transfer and the energy conservation will give the condition

$$-\frac{1}{\omega_\mathrm{p}}\frac{\mathrm{dI}_\mathrm{p}}{\mathrm{dz}} = \frac{1}{\omega_\mathrm{s}}\frac{\mathrm{dI}_\mathrm{s}}{\mathrm{dz}} = \frac{1}{\omega_\mathrm{i}}\frac{\mathrm{dI}_\mathrm{i}}{\mathrm{dz}}. \tag{3.22}$$

This relation is called the Manley-Rowe equation, and describes the energy flow between the interacting fields [27].

By integrating Eq.(3.21) the signal single-pass amplification for a parametric device of length L can be written as

$$\frac{I_{s(L)}}{I_{s(0)}} = 1 + \Gamma^2\frac{\sinh^2\left(L\sqrt{\Gamma^2 - \left(\frac{\Delta k}{2}\right)^2}\right)}{\Gamma^2 - \left(\frac{\Delta k}{2}\right)^2}, \tag{3.23}$$

by assuming the incident signal wave is weak and the depletion of the pump is low. Here the parameter Γ^2 is defined as

$$\begin{aligned}\Gamma^2 &= \kappa I_p,\\ \kappa &= \frac{8\pi^2 d_{eff}^2}{\epsilon_0 c n_p n_s n_i \lambda_s \lambda_i}.\end{aligned} \tag{3.24}$$

This can be simplified by assuming $\Gamma L \gg 1$, which gives the approximation:

$$\frac{I_{s(L)}}{I_{s(0)}} = \frac{1}{4}\exp\left(2L\sqrt{\Gamma^2 - \left(\frac{\Delta k}{2}\right)^2}\right), \tag{3.25}$$

In the above equations plane waves are assumed. For the nonlinear interactions to take place is it convenient to work with strong focused laser beams, to reach high energy densities. However, as long as the PPKTP crystal is placed within the Rayleigh range of the beam plane waves can be assumed. What ultimately limits the focusing of the beam, in this work, is the damage threshold of the components. However it is desirable to match the focused beam with the mode of the resonator or, with the aperture of the crystal, making the Rayleigh range longer than the crystal, and the plane wave assumption is therefore valid.

The pump energy threshold of for an OPO operating with nanosecond pulses can be written as [28]

$$\mathcal{E}_{th} = \frac{0.6\left(\omega_p^2 + \omega_s^2\right)}{\kappa L^2}\left[\frac{25l}{\tau c} + \frac{1}{2}\ln\frac{2}{R(1-A)}\right]^2, \quad \textbf{(3.26)}$$

where R is the reflectivity of the output coupler, A accounts for the losses in the cavity, τ is the FWHM of the pulse length, L crystal length, l optical cavity length, ω_p and ω_s the mode radius of the pump and signal respectively. When the threshold is reached and the OPO is operating, the signal and idler will deplete the pump so that the gain and losses in the process are equal.

As a measure of how well the OPO is working both the pump depletion and the efficiency of the OPO can be used. The nonlinear loss of the pump in the process is what is called the pump depletion. It is measured by comparing the total loss of the pump in the process to the linear loss of the pump below oscillation threshold. By letting $\mathcal{E}^*$ denote the measured energy below threshold, the pump depletion can be written

$$\eta_{depl} = 1 - \frac{\mathcal{E}_p^{out}}{\mathcal{E}_p^{in}}\frac{\mathcal{E}_p^{*in}}{\mathcal{E}_p^{*out}}. \quad \textbf{(3.27)}$$

The efficiency of the OPO can be calculated from

$$n_{eff} = \frac{\mathcal{E}_s^{out} + \mathcal{E}_i^{out}}{\mathcal{E}_p^{out}}. \quad \textbf{(3.28)}$$

If the energy of the idler is not measured, it can be calculated as $\mathcal{E}_i = \mathcal{E}_s\lambda_s/\lambda_i$ from the Manley-Rowe relation, Eq.(3.22).

In an ideal OPO every depleted pump photon is transferred by the nonlinear process into one signal and idler pair of photons. So, the pump depletion should equal the efficiency of the OPO. In reality there are often losses due to scattering and diffraction in the resonator so the pump depletion is usually higher than the efficiency of the OPO.

The desired wavelengths in the process can be obtained from fabricating periodically poled KTP crystals. From Eq.(3.15) the period of the ferroelectric grating for the desired wavelengths can be calculated from

$$\Lambda = \frac{1}{\frac{n_p}{\lambda_p} - \frac{n_s}{\lambda_s} - \frac{n_i}{\lambda_i}}. \quad \textbf{(3.29)}$$

By that the gain curve for the process can be engineered to obtain desired wavelengths in the OPO. The refractive index of KTP can be found in Fradkin et al. [29] and Kato and Takaoka [30] where it has been determined experimentally.

If it is desirable to move the gain curve, and hence the spectrum, of the OPO, this can be done in several ways. In this work this is mainly done by temperature tuning. The gain curve is then adjusted by changing the refractive index and the length of the grating period by adjusting the temperature of the crystal. Eq.(3.14) can be differentiated with the respect to temperature and the tuning rate for the signal frequency is then given by

$$\frac{d\upsilon_s}{dT} = \frac{1}{c\left(\frac{1}{v_{gs}} - \frac{1}{v_{gi}}\right)}\left[\upsilon_p \frac{dn_p}{dT} - \upsilon_s \frac{dn_s}{dT} - \upsilon_i \frac{dn_i}{dT} - \frac{c}{\Lambda}\alpha\right], \quad \textbf{(3.30)}$$

where α is the thermal expansion and ν_g is the group velocity. The temperature derivatives of the refractive index can be found in Emanueli and Arie [31].

Another way to adjust the gain curve is to change the angle with which the pump beam is incident on the crystal. That will then change the length of the grating in the direction of the pump beam

The bandwidth of an OPG can be calculated from Eq.(3.25). Combining the value of Δk when the single pass amplification, Eq.(3.23), is reduced to half its maximum values, with the detuning of the signal frequency this phase mismatch results in the bandwidth of the OPG (off degeneracy) being

$$\Delta\nu = \frac{2\ln(2)^{1/2}}{\pi}\left(\frac{\Gamma}{L}\right)^{1/2} \frac{1}{\left|\frac{1}{v_{gs}} - \frac{1}{v_{gi}}\right|}. \quad \textbf{(3.31)}$$

When the OPG is placed within a cavity and by that turned into an OPO this will affect the spectrum of the process. The multiple passes in the crystal and the cavity will narrow the spectrum, since the gain curve will multiply with itself. Also, when working with a standing wave cavity, as in this work, the longitudinal modes of the cavity might be imposed on the spectrum. However, when working with pulsed OPOs the mode buildup might be limited by the bandwidth of the pump beam.

Since the nonlinear process is very fast and information such as the phase of the pumping beam is transferred to the signal and idler one can expect that the signal and idler will inherit the properties of the pump beam. Properties such as bandwidth and M^2, or rather temporal and spatial coherence, will ultimately be transferred to the created signal and idler. There are, as will be shown, however means to improve the coherence of the generated beams.

4 OPO experiments

In this chapter the experiments carried out in this work are presented and analyzed. The purpose of the experiments was to investigate the possibilities of enhancing the temporal and longitudinal coherence of mid-infrared parametric devices.

First an optical parametric oscillator was designed and a highly coherent laser was used as pump source. By properly matching the TEM_{00} mode of a stable resonator with the focused pump beam, highly coherent beams in the mid-infrared part of the spectrum could be generated. Generally the properties of the pump source, such as spectral bandwidth and beam quality factor, are transferred to the generated beams.

Highly coherent lasers, i.e. lasers operating in single transversal and longitudinal mode, are expensive and generally consist of large and sensitive systems. Therefore an investigation of using a multimode laser as pump source was done. Lasers operating in multiple transversal and longitudinal modes are substantially cheaper than single mode lasers and can generate large energies in compact arrangements. These properties make them attractive to be used as pump sources. Since the properties of the pump beam are transferred to the generated beams, it was of interest to investigate how the spatial and temporal coherence could be improved. Therefore it was of interest to investigate pumping nonlinear processes by employing Bessel beams. A multimode pump source was therefore used to pump OPG and OPO when pumping the process both by Gaussian and Bessel beam.

4.1 OPO with a stable cavity

One way of generating highly coherent beams in the mid-infrared spectrum is to use an optical parametric oscillator, OPO, pumped by a highly coherent laser and controlled by a stable cavity. The highly coherent laser pump source makes it possible to generate highly monochromatic signal and idler waves while the stable cavity provides feedback for the signal wave and with proper mode matching with the focused pump beam makes it possible to generate signal and idler waves that are spatially highly coherent.

A seeded Q-switched all diode-pumped Nd:YAG laser and amplifying system operating in single longitudinal-mode at 1064.4 nm is used in this experiment. It has a 12 ns long pulses and 100 Hz repetition rate. Since it is seeded it operates in a single longitudinal mode and has a beam quality factor $M^2 \approx 3$. The laser has a pulse energy of 241 mJ. The pump energy was controlled by using a polarizing beam splitter and a half-waveplate. The pump beam was focused with three lenses in order to have a small focus and a Rayleigh range of around 10 mm. The size of the focus was measured with the knife-edge method to be approximately 70 μm. However, the beam suffered from some astigmatism, locating the horizontal and vertical foci at different positions along the optical axis.

An PPKTP crystal with a ferroelectric period of 36.4 μm was chosen to obtain quasi phase matching at the desired wavelengths for the signal of 1596.6 nm and the idler of 3193.2 nm. The crystal was 10 mm long and of 1 mm thickness. The theoretical value of the period can be calculated using Eq.(3.15) to be 36.51 μm. However, preliminary experiments showed this period provided the wrong wavelengths, and moreover temperature tuning to the desired

wavelength was not possible. Therefore the period was adjusted to 36.4 μm and the desired wavelengths could be reached. The theoretical value of the grating period did not generate QPM for the desired wavelengths since it is determined from Sellmeier equations from Fradkin et al. [29] and Kato and Takaoka [30] with Eq.(3.14). These Sellmeier equations are not measured at the wavelengths that are generated in this work and the difference between them close to degeneracy is rather large [32]. Measurements by Yoshida [25] have shown KTP crystals have a damage threshold of approximately 20 J/cm^2. However, the damage threshold varies depending on wavelength, pulse length and several other parameters. To not damage the crystals, the limiting pump power was therefore calculated with a maximum fluence of 1 GW/cm^2, corresponding to approximately 10 J/cm^2. Moreover, the crystal did not have any anti reflection coating for any of the involved wavelengths.

A resonator was simulated with the help of the program Winlase [33]. The purpose of the simulation is to calculate the beam radius of the fundamental mode of the Gaussian beam supported by the cavity. With that knowledge it is then possible to pump an area smaller than the lowest order Gaussian mode in order to support that mode in the cavity. It is desirable to pump an area as big as possible to lower the energy fluence in the crystal. A tightly focused beam will give high energy fluence, and ultimately damage the crystal. However, pumping a too large area of the crystal will support higher order transversal modes in the cavity, which will decrease the spatial coherence of the beam. The focused pump beam and the lowest order Gaussian mode of the simulated are shown in Figs. 4.1. The TEM_{00} mode at the signal wavelength of the resonator is diffracting slower than the focused pump beam. Comparing the Rayleigh range of the focused pump beam and the TEM_{00} mode of the resonator, shows the Rayleigh range of the pump beam is about half as long as that of the focused pump beam. That is, due to the beam quality factor M^2~3 of the pump beam the pump beam is diffracting faster than the TEM_{00} mode of the resonator.

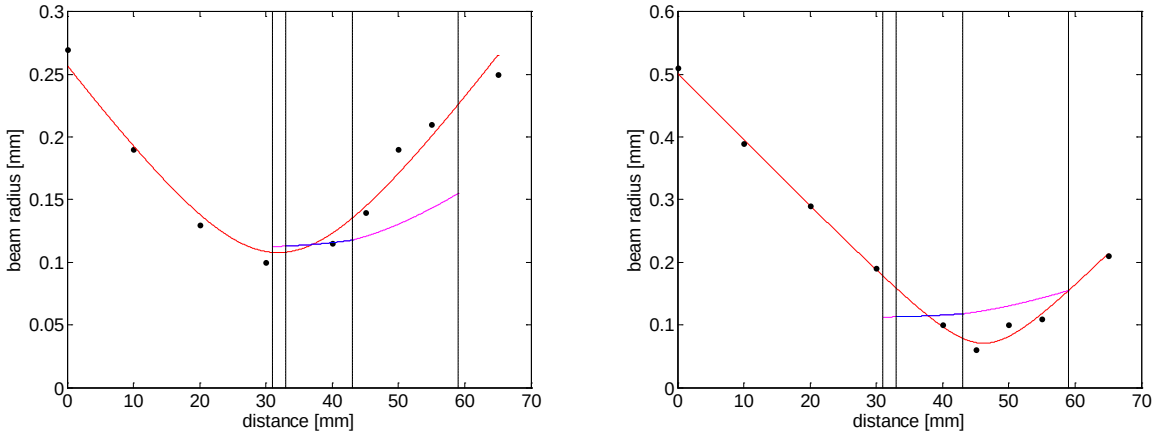

(a) (b)

Figure 4.1: The focused pump beam (red) with the simulated cavity radius (magenta) and the crystal position (blue). Dashed lines indicate the position of mirrors and crystal end faces for a better overview. In (**a)** is the horizontal plane displayed and in (**b)** the vertical plane

A plano-convex stable cavity was built with dielectric mirrors in order to support the lowest order Gaussian mode, according to the simulations in Fig. 4.1. The input coupler in the resonator was a dielectric mirror with a reflectivity close to 100%, for the signal and a radius of curvature (ROC) of 50 mm. The output coupler was a flat dielectric mirror with a reflectivity of 56% for the signal. The length of the cavity was 28 mm. A PPKTP crystal rested on a copper black and the temperature of the copper block, and hence the crystal, was controlled by a Peltier element.

This setup gave a beam radius of the fundamental Gaussian mode within the cavity of approximately 100 µm. Another option would have been a concentric/confocal cavity since it would have a nicer overlap with the focused pump beam. That would require a longer cavity, and would therefore result in a higher threshold of the parametric process. A schematic picture of the plano-convex setup is shown in Fig. 4.2.

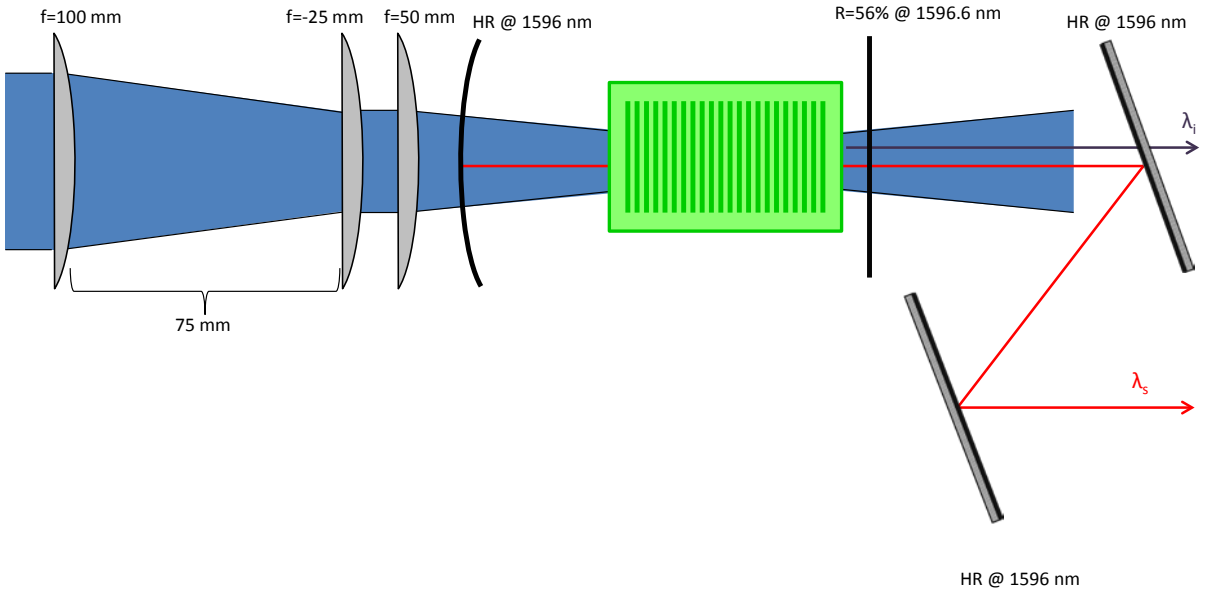

Figure 4.2: Sketch of the setup pumped with a Gaussian beam and using a stable cavity. Blue, red and violet lines are representing the pump, signal and idler, respectively. The length of the cavity was 28 mm.

Fig. 4.3a displays the efficiency and the pump depletion of the OPO and Fig. 4.3b displays the output energy of the signal wave. The efficiency is calculated with Eq.(3.28) and Eq.(3.22) using the measured energy of the input pump beam and the signal beam. Measurements of the transmitted pump beam were made after the first mirror in the filtering stage, and the measured data could be used in Eq.(3.27) to calculate the pump depletion of the process. The OPO has an oscillation threshold at slightly below 0.3 mJ of pump pulse energy. The efficiency increases slowly and reaches a maximum of 15% three times above threshold and the maximum output energy of the signal wave is 0.9 mJ. The output energy was only measured to slightly above three times the threshold to not risk damaging the crystal. Also, higher above threshold losses in the OPO due to parasitic processes and back conversion will increase causing the efficiency to decrease. Only half of the depleted pump is converted to signal and idler waves, suggesting the losses in the cavity are rather high. Since the crystal is uncoated, it reflects about 10% of both the signal and idler waves. There can therefore be

back conversion in the backward direction. The generated signal wave can also act as a pump source for a second parametric process. Calculations show that phase matching is obtained when 2.83 µm and 3.66 µm are generated when the signal wave is used as pump source. The generated idler will act as a seed for the second parametric process. The down conversion will thereby transfer energy from the signal wave into the idler. However, the powers at the idler wavelength are not measured and thereby not providing a solid proof. Since the interacting waves are co-propagating Also, the fluctuations in the pulse energies are rather big, about 10-20%. However, the purpose of this OPO is to generate a highly coherent beam, so the efficiency is not the main concern.

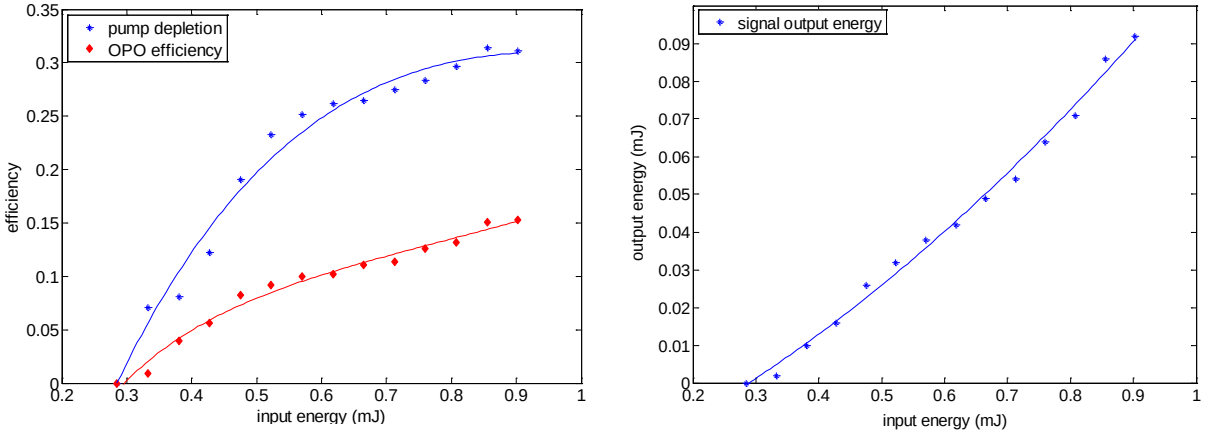

(a) (b)

Figure 4.3: Measured values combined with trend lines for **a)** The efficiency and the depleted pump of the OPO **b)** The output energy of the signal of the OPO.

Spectra of the signal were recorded with an optical spectrum analyzer (OSA) which has a resolution bandwidth of 0.1 nm. When recorded with the OSA the spectrum showed a very distinct behavior of regular peaks due to the etalon effect caused by the close spacing between the crystal and the output coupler. The spectrum was recorded at several different temperatures. The central wavelength at each temperature is displayed in Fig. 4.4, together with simulated signal wavelength as a function of temperature with Sellmeier equations from Fradkin [29] with temperature correction from Emanueli and Arie [31], and temperature corrected Sellmeier equations from Kato and Takaoka [30]. The measured data follows the simulated curves, even if it is slightly oscillating. The discrepancy between the measured data and theoretical curves might be due to the fact that none of the theoretical curves are measured at this wavelength. Also, the desired wavelengths are rather close to degeneracy of the pump beam. Close to degeneracy, i.e. generating 2 µm from a 1 µm pump beam, the calculated values for the domain grating period differ significantly depending on which reference is used for the refractive index. This might also explain why the theoretical value of the QPM period for the desired signal and idler wavelength pair was outside of the temperature tuning range. The desired wavelengths of the signal and idler were obtained at 50˚C.

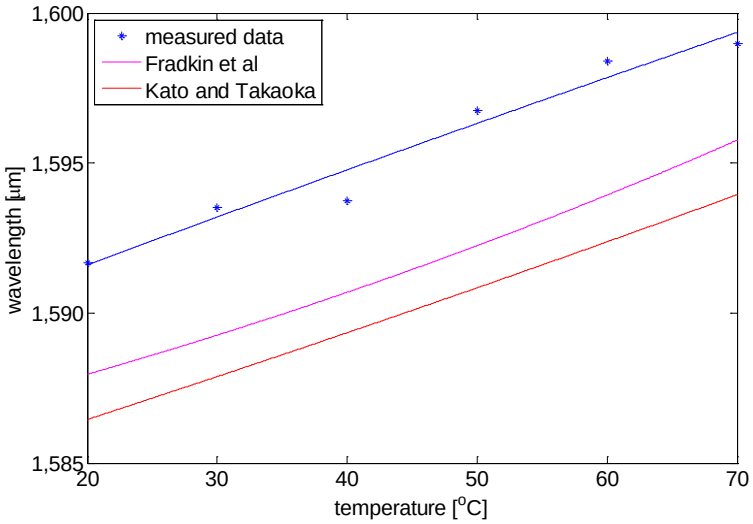

Figure 4.4*:* The wavelength of the signal as a function of the temperature of the crystal. Measured data, star and trend line, is displayed together with theoretical curves calculated from [29] and [30]

The spectra of the signal and idler in the OPO were recorded at 50˚C by using a lock-in amplifier and a spectrometer (JobinYvoniHR 550) with a PbSe detector, and are displayed in Figs. 4.5. When the spectrum of the idler wave was measured, a 2 µm band-pass filter was used to block the pump and signal waves. The signal wave could otherwise show up as artifacts in the spectrum, making it more difficult to interpret. The signal has a central peak at 1595.9 nm and a FWHM of 0.2 nm. Two small side peaks can be observed in the spectrum located approximately 1nm apart from the central peak. A spacing of approximately 1nm corresponds to a Fabry-Perot etalon with a width of approximately 1.5 mm. This etalon effect is a result of the crystal being placed approximately 1.5 mm from the output coupler. Since the crystal is not anti-reflection coated for any of the involved wavelengths this phenomenon will occur. The spectrum of the idler has its central peak at 3192.9 nm and a FWHM of 0.5 nm, corresponding to 14 GHz. The resolution of the spectrometer is about 19 GHz, meaning that the spectra might be narrower than the resolution of the spectrometer. This spectrum shows only one side peak with a spacing of 1.3 nm, which corresponds to 38 GHz. This side peak is an effect of the small peaks in the spectrum of the signal. The intracavity Fabry-Perot etalon will allow the signal to be resonant at certain resonant frequencies. The small side peaks in the signal will therefore give rise to small side peaks in the idler spectrum as well, which wavelength can be calculated by the Manley-Rowe relation. Over all, the OPO show a high temporal coherence, which is an effect of using a single longitudinal mode pump laser.

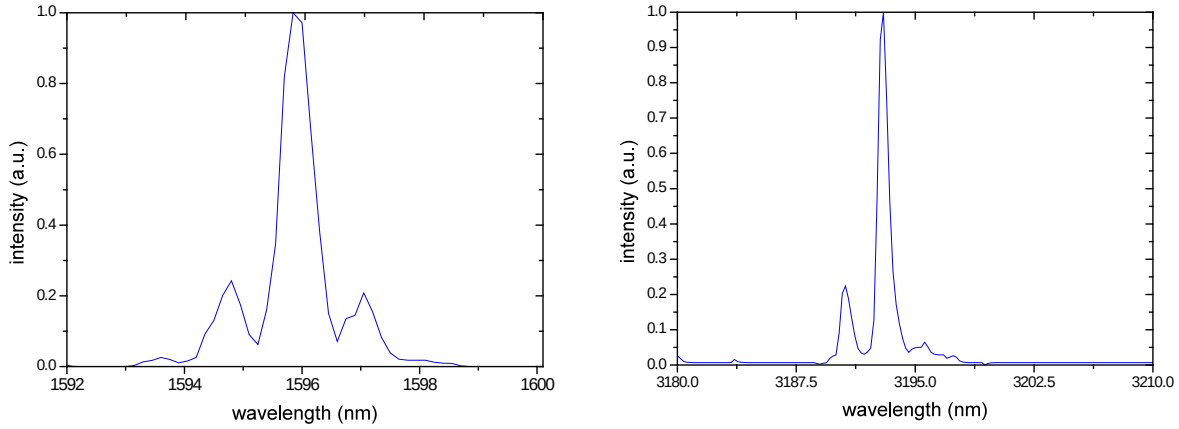

(a) (b)

Figure 4.5*: a)* The spectrum of the signal wave in the OPO at 50˚C. **b)** The spectrum of the idler wave in the OPO at 50˚C

The M^2 was calculated from measurements of the beam radius at several positions after a lens with focal length of 150 mm. The beam radius was measured with the knife-edge method. A fitting of Eq.(2.6) to the measured data gives M^2_{hori}=1.3 and M^2_{vert}=1.7. The measured data and the result of the fitting are shown in Figs. 4.6. The slightly worse spatial coherence in the vertical direction is an effect of the astigmatism of the pump beam. Due to the astigmatism it is not possible to mode match both the vertical and horizontal direction perfectly. This will show as the spatial coherence being slightly worse in one direction. As can be seen in Figs.4.6 is the mode matching not perfect since the Rayleigh range, the length of the focus, is a bit too short to obtain perfect mode matching simultaneously for the horizontal and vertical direction, and the spatial coherence will therefore decrease slightly. The Rayleigh range is however a property linked to the M^2 of the pump beam, which is difficult to improve. However, a M^2 around 1.5 indicates a spatial coherence which is high enough to fulfill the requirements stated in the introduction.

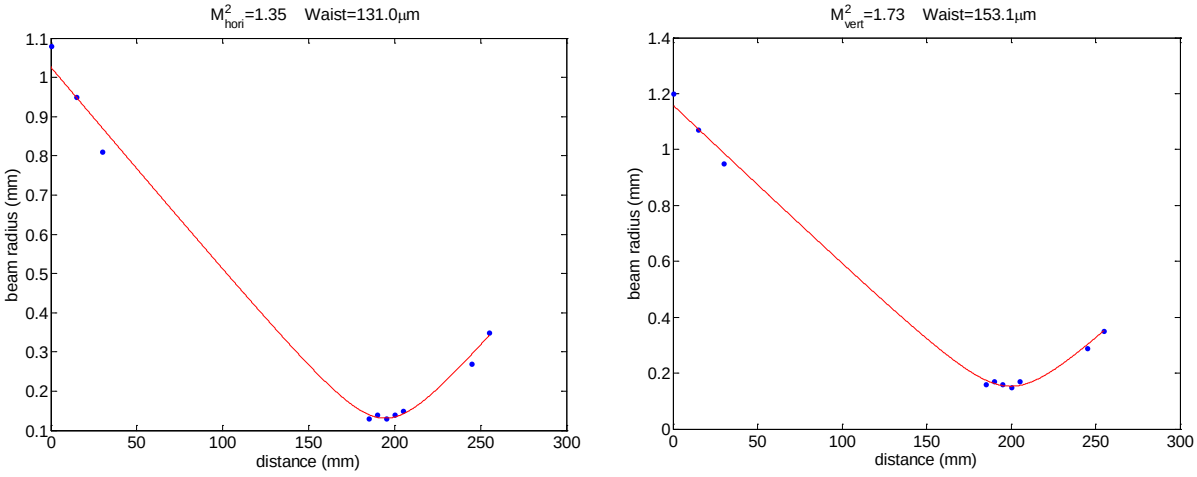

(a) (b)

Figure 4.6*:* Measured beam radii at several distances from the lens are shown by blue point and the fitting of the measured data to Eq.(2.6) is shown by the red line. The right graph **a)** shows the horizontal measurements and the left graph **b)** the vertical measurements.

4.2 Parametric processes pumped by a Gaussian and a Bessel beam

The purpose of this set of experiments is to investigate the difference of beam quality of the output beam when pumping a parametric process with a transverse Bessel intensity distribution rather than a Gaussian one. Pumping the nonlinear process with a Bessel beam might improve the beam quality and the spectral quality of the output signal when a pump beam of poor spatial and temporal coherence, i.e. a pump beam with a rather high beam quality factor, M^2, and a broad spectrum, is used. OPG and OPO were investigated with both pump configurations. The investigation of the OPG provided understanding of how the coherence is affected by the various pump configurations, unhindered by the averaging effects of the resonator.

Throughout these experiments a flashlamp-pumped Q-switched Nd:YAG laser was used to pump the parametric process. The laser provided 6.5 ns (FWHM) long pulses at 20 Hz repetition rate. It operates in longitudinal-multimode oscillations around a center wavelength of 1064 nm. The beam quality factor, M^2, was measured to be 5.

A PPKTP crystal with a period of 36.4 μm was used to generate the desired wavelength pair of 1596.6 nm and 3193.2 nm. The same crystal described in Chap. 4.1 was used. When pumping the crystals with a conical beam, which is the case when pumping with a Bessel beam, the phase-matching conditions will change, as seen in Chap. 3.2. This will slightly change the required grating period from the collinear case. This change is however small enough to be within the wavelength range tunable by temperature.

In the OPO setups a Fabry-Perot cavity with two plane mirrors was used as resonator, and was singly resonant for the signal wave. The input coupler was coated for high reflectivity (>99%) at the signal wavelength and low reflectivity (<5%) at the pump wavelength. The coating of the output coupler provided a reflectivity of about 43% at the signal wavelength. The length of the cavity was 24.5 mm. After the resonator (or crystal when working with the OPG) a filtering stage was constructed consisting out of two dielectric mirrors, which were highly reflective for the signal wave, with the purpose of separating out the signal wave from the remaining pump wave to make individual measurements on the signal possible.

4.2.1 Pumping of OPG by a focused Gaussian beam

To investigate the gain properties of the crystal and how the resonator affects the parametric process was an OPG set up. The OPG was pumped by a Gaussian beam that was focused with a plano-convex lens with 50 mm focal length. The beam waist of the pump beam was measured to be 75 μm and the Rayleigh range was approximately 10 mm. The crystal was placed within the Rayleigh range, since one can assume the laser beam to propagate as plane waves within this distance. Fig. 4.7 is a schematic picture of the setup. The crystal rested on a copper block and the temperature was kept to 50°C, just as for the stable cavity OPO, to fulfill the phase matching conditions for the desired wavelengths.

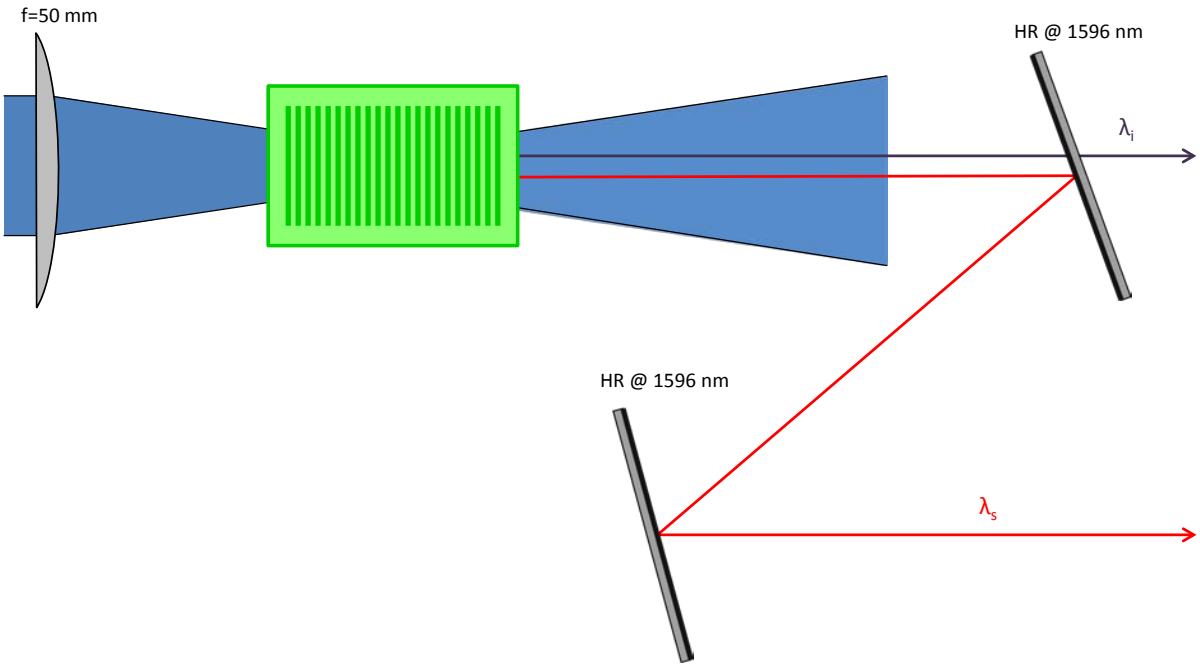

Figure 4.7: Sketch of the setup pumped with a Gaussian beam focused by a regular lens. Blue, red and violet lines are representing the pump, signal and idler.

The output energy of the signal is shown in Fig. 4.8b and the efficiency and pump depletion of the OPG are shown in Fig. 4.8a. The OPG has its threshold at 0.5 mJ of pump pulse energy. Due to the risk of damaging the crystal the output power was only measured to be slightly three times above threshold. That is, when the pump input power is about 1.1 mJ. The efficiency three times above threshold is 15% and the pump depletion about 24%. The depletion of the pump saturates about two times above threshold. In an OPG all of the depleted pump should be transferred into the generated signal and idler wave. Therefore the efficiency and the pump depletion are supposed to be equal. In these graphs they are not. One possible explanation is that the generated signal acts as pump wavelength for a second parametric process. Calculations of the QPM shows a second signal and idler pair, at 2.8 µm and 3.66 µm respectively, that is phase matched for the employed grating period when using the desired signal wave at 1596 nm as a pump source. Since all interacting waves are co-propagating, the generated idler will act as a seed for the second parametric process. Despite not being perfectly phase matched, the second parametric process will have gain and transfer energy from the signal wave to the idler wave. This will deplete the measured signal and can account for the discrepancy between the measured depleted pump and the efficiency of the process. This cascaded process is possible since all interacting beams are co-propagating, that is, propagating in the same direction and therefore enabling interactions between the various beams. Also, the measured intensity fluctuates about 10-20% for all measured values, and hence might the discrepancy between the depleted pump and the efficiency of the process be smaller than indicated.

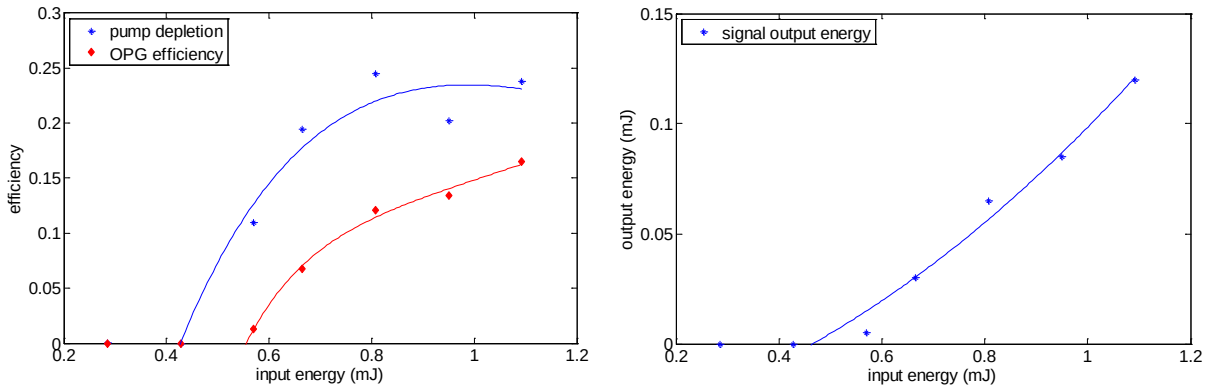

(a) (b)

Figure 4.8: a) The efficiency and pump depletion of the OPG. **b)** The output energy of the signal of the OPG.

Fig. 4.9 displays the spectrum of the OPG at two times above threshold recorded with an OSA at 50°C approximately 3 times above threshold. The spectrum has its center at 1596.5 nm and a FWHM of 4.5 nm. The broad spectrum is an effect of the multi mode nature of the pump beam. The spectrum of the idler wave is not measured since the OSA only has a range of 380-1700 nm. The broad spectrum of the pump, due to the multiple longitudinal modes, is transferred to the signal and idler waves.

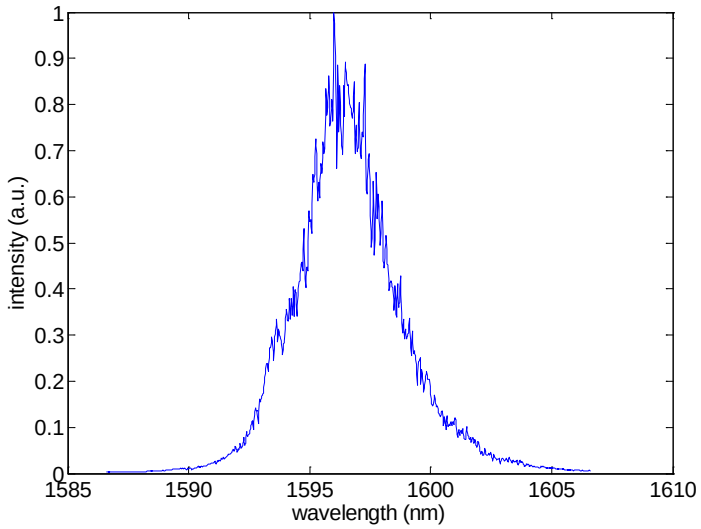

Figure 4.9*:* The spectrum of the signal wavelength in the OPG at 50˚C.

The M^2 was calculated from measurements of the beam radius at several positions after a lens with focal length 70 mm. The beam radius was measured with the knife-edge method. A fitting of Eq.(2.6) to the measured data gives M^2_{hori}=5.8 and M^2_{vert}=4.4. The measured data and the result of the fitting are shown in Figs. 4.10. This resembles the properties of the pump beam, which is expected. The multi mode nature of the pump will result in the pump photons having of a lot of different momenta (wave vectors) and the difference will be transferred to the signal and idler waves.

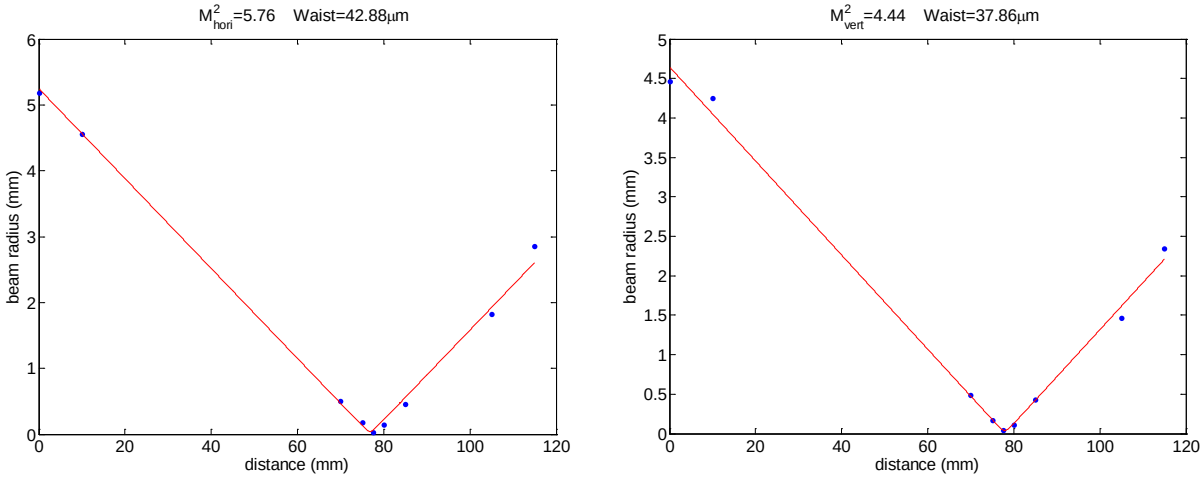

(a) (b)

Figure 4.10: Measure beam radii at several distances from the lens are shown by blue point and the fitting of the measured data to Eq.(2.6) is shown by the red line.The right graph **a)** shows the horizontal measurements and the left graph **b)**the vertical measurements

4.2.2 Pumping of OPG by a Bessel beam

Just as for the Gaussian pumped process is it of relevance to investigate the gain properties of the PPKTP crystal when being pumped with a conical beam. This will give insight to what effects the non-collinear phase matching has and how a resonator can be used to exploit these effects.

A transverse Bessel intensity was created with the help of an axicon with a prism angle $\alpha=1°$. This top angle gives a beam radius of approximately 30 μm, approximated using Eq.(2.20). The crystal was placed in the focal line of the axicon at a distance of approximately 80 mm. The crystal rested on a copper block and its temperature was controlled and kept at 55˚C to fulfill the phase matching conditions for the desired signal and idler wavelength pair. A schematic picture of the setup is shown in Fig. 4.11.

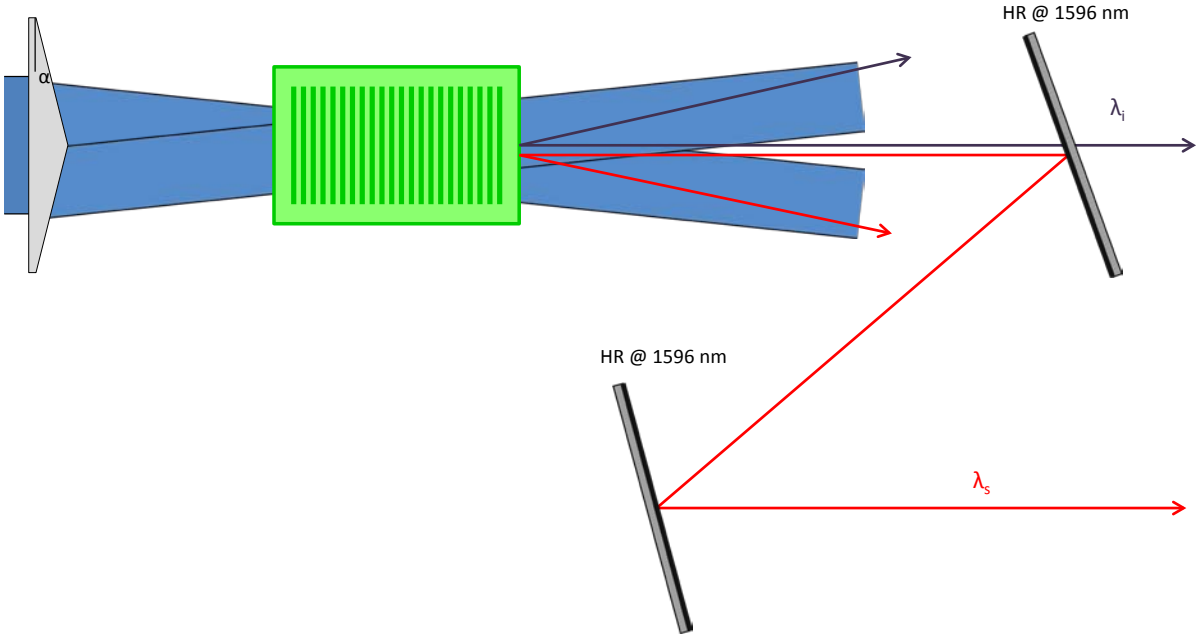

Figure 4.11: Sketch of the setup with blue, red and violet lines representing the pump, signal and idler.

The efficiency and the pump depletion of the OPG are depicted in Fig. 4.12a and the output power of the signal wave is depicted in Fig. 4.12b. The threshold of the parametric process was measured to 2.2 mJ of input pulse energy. The input pump pulse energy was limited to 4.5 mJ to avoid damaging the crystal. The efficiency 2 times above threshold is 6%, while the pump depletion is 14% with a maximum output power of 0.16 mJ of the signal wave. There is, however, no sign of depletion saturation at 2 times above threshold. The measurement is, in fact, restricted by the limited input pump energy. In the Gaussian pumped OPG saturation was already apparent as an effect of the noncollinear interactions. Since all interacting beams are propagation in different directions there will be no back conversion in the forward direction. Only half of the depleted pump is transferred in to signal and idler. As described in Chap 3.2, there are two possible phase matching options which results in high parametric gain. In one of the possible high gain possibilities, the signal wave is propagating in a cone with an angle larger than the angle of the conical pump beam, and the idler is propagating along the optical axis. That might explain why the efficiency is not equal to the depleted

pump. About half of the pump which is depleted is transferred into the signal and idler pair in which the idler propagates along the optical axis and the signal propagates in a cone and is therefore not detected by the power meter, after the separation stage, hence the discrepancy between efficiency and pump depletion.

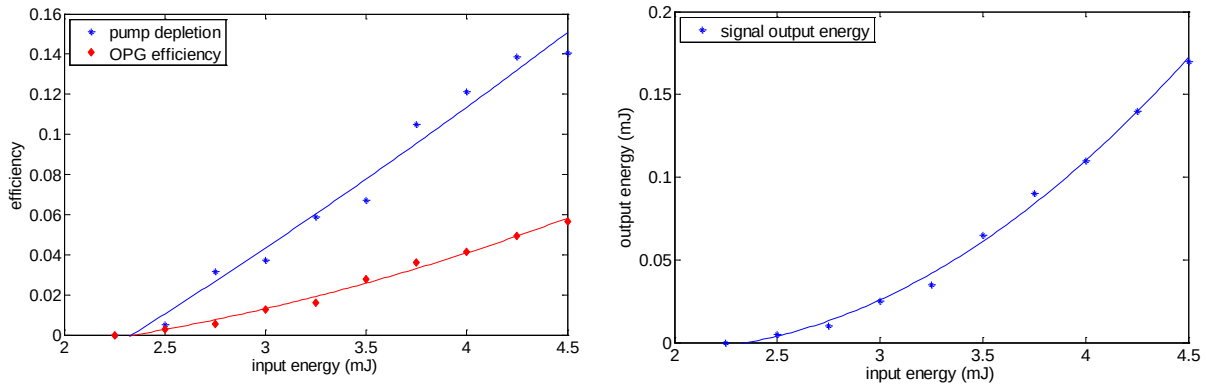

(a) (b)

Figure 4.12*: a)* The efficiency and depleted pump of the OPG. **b)** The output power of the signal wave of the OPG.

Fig. 4.13 shows the spectrum of the signal wavelength in the OPG at two times above threshold when kept at 55 °C, which is recorded with an OSA, where the desired wavelength of the signal was obtained. The OPG has a center wavelength of 1596.7 nm and bandwidth of 2.8 nm at FWHM, which corresponds to an idler wavelength of 3189.2 nm, calculated using Eq.(3.7). The idler is, however not measured, due to the limited wavelength range of the OSA. As seen in Chap. 3.2 the QPM when using Bessel beams will give rise to two resonant pairs with high parametric gain for each period length of the ferroelectric grating. This, when not controlled by a resonator, will broaden the spectrum of the parametric process by allowing several different processes to take place. The main factor influencing the spectral width is the diffraction free propagation length, i.e. the length of the focal line, which in turn is determined by the coherence radius of the beam and the prism angle, α, of the axicon. This is the length of the nonlinear process in which the parametric gain can be tied to the spectral width.

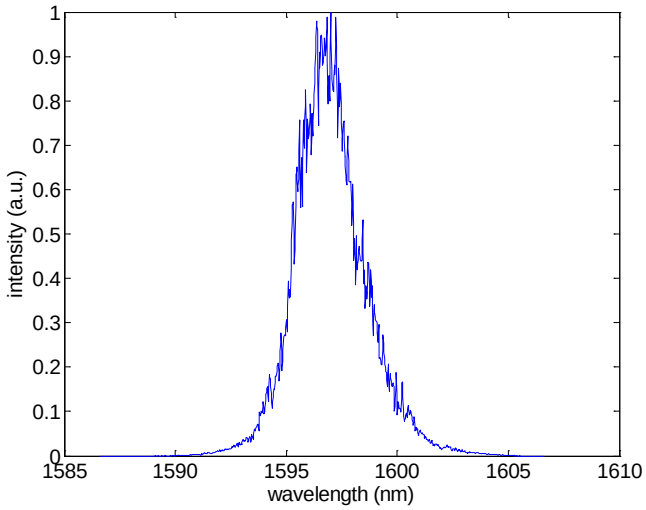

Figure 4.13: Spectrum of the Bessel pumped OPG at 55 ˚C. The temperature difference compared to the OPO in previous section can be accounted for by the lack of a resonator and the orientation of the crystal.

After the filtering stage the signal beam was focused by a lens with focal length 70 mm. The beam radius after the lens was measured at several positions on the optical axis. The measurement was done with the travelling knife-edge method and Eq.(2.6) was fitted to the measured values. Figs. 4.14 display the measured beam radii and the fitting of Eq.(2.6). M^2_{hori}=2.5 and M^2_{vert}=2.5 were obtained in this setup. This result is lower than for the Gaussian pumped OPG, suggesting that the noncollinear phase matching improves the spatial coherence as well as the temporal coherence. The interference in the Bessel beam provides an automatic selection of the spatially coherent parts of the pump beam, which will be transferred to the generated waves. The spatial coherence is therefore improved by the limitation on how high gain can be obtained in the nonlinear process.

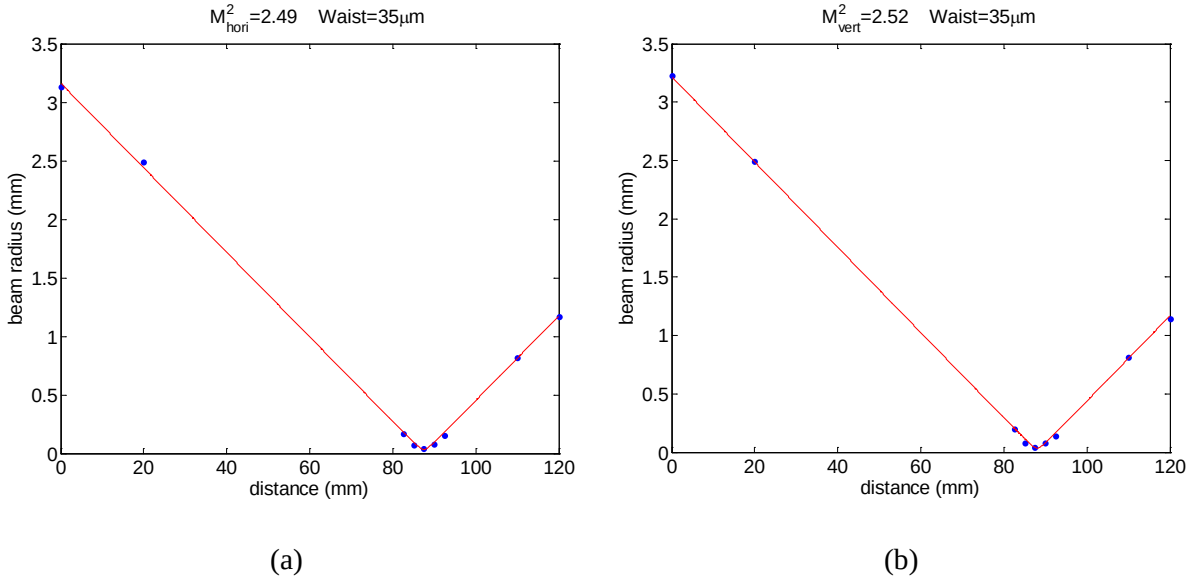

(a) (b)

Figure 4.14: Measured beam radii at several distances from the lens are shown by blue point and the fitting of the measured data to Eq.(2.6) is shown by the red line. The right graph **a)** shows the horizontal measurements and the left graph **b)** the vertical measurements.

4.2.3 Pumping of OPO by a focused Gaussian beam

In this setup an OPO was pumped by a Gaussian beam which was focused with a plano-convex lens of focal length of 50 mm, similar to the Gaussian pumped OPG. The beam waist of the pump beam was measured to be 75 µm and the Rayleigh range was approximately 10 mm. The crystal was placed within the Rayleigh range, since one can assume the laser beam to propagate as plane waves within this distance. The maximum input power used was limited to 2 mJ which did not damage the crystal. The same crystal as for the OPG (described in Chap. 4.2.1) was used. A schematic picture of the setup is shown in Fig. 4.15.

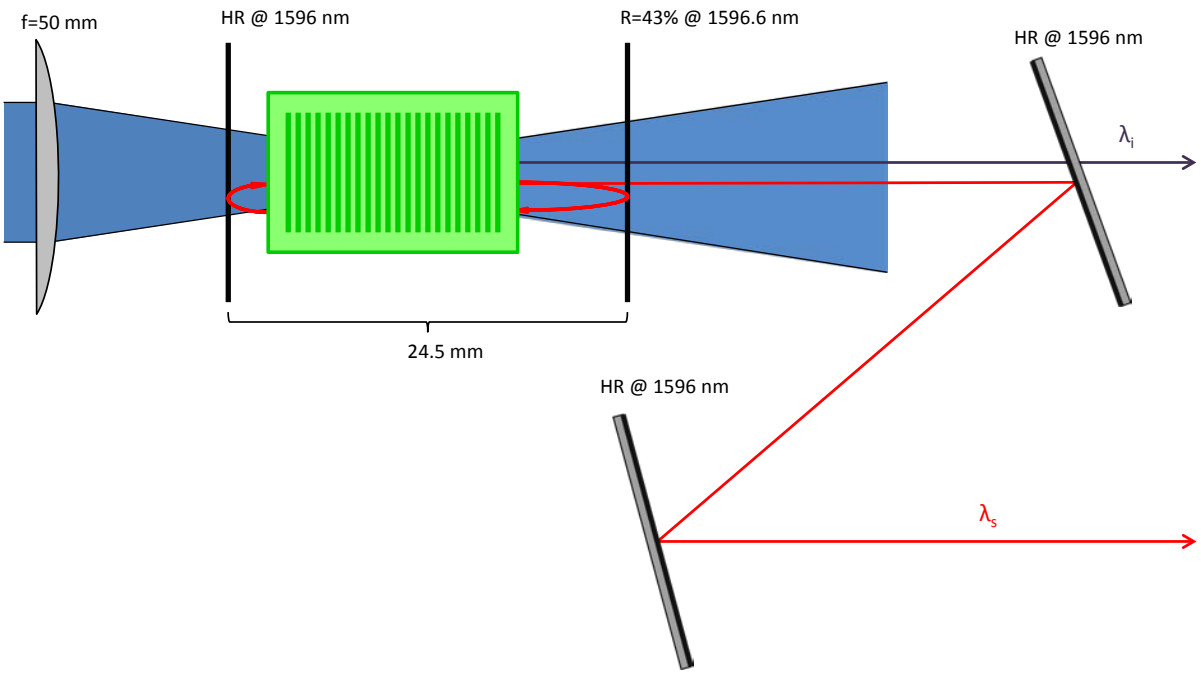

Figure 4.15: Sketch of the setup pumped with a Gaussian beam focused by a regular lens. Blue, red and violet lines are representing the pump, signal and idler. The length of the cavity was 24.5 mm.

The efficiency together with the pump depletion of the OPO are shown in Fig. 4.16a and the output energy of the signal wave is displayed in Fig. 4.16b. The threshold of the OPO is at 0.2 mJ of pump pulse energy. The maximum output pulse energy of the signal wave is measured to be 0.18 mJ. The OPO reaches its maximum efficiency of about 18% with pump depletion of about 27% at pump pulse energies 3 times above the threshold value, which is higher than for the Gaussian pumped OPG. The efficiency then decreases slightly, even though the pump depletion increases, due to losses from parasitic effects and back conversion from the signal and idler to the pump wave. Among other things, SFG between the pump and the signal was observed. Also observed was SFG between the signal and the parasitic SHG of the pump resulting in radiation at a wavelength of 399 nm. These SFG processes are, however, operating at so low powers they are not measurable. One explanation for the discrepancy in efficiency and the pump depletion might be the signal wave acting as a pump source for down conversion. Calculations show that phase matching is obtained for generating the wavelengths

at 2.66 µm and 3.66 µm when using the signal wave as a pump source. The collinear phase matching makes the idler seed a second parametric process, transferring energy from the signal wavelength into the idler wavelength. This will deplete the generated signal wave at 1596 nm, and will be shown as a discrepancy between the efficiency and the depleted pump.

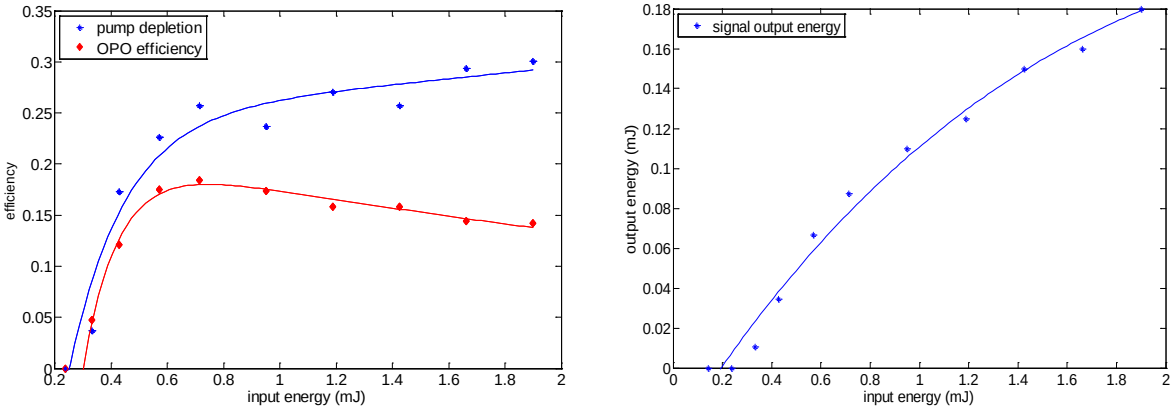

(a) (b)

Figure 4.16: a) Efficiency and depleted of OPO pumped with a focused Gaussian beam. **b)** Output power of signal wave.

The spectrum of the signal in this OPO is shown in Fig. 4.17a. Fig. 4.17b shows the spectrum with the crystal turned a few degrees in order to remove etalon effects. The spectra have their central peaks at 1596.3 nm and 1597.2 nm respectively, so the turning of the crystal also slightly changes the central wavelength. The peaks in Fig. 4.17a have a FWHM of 0.1 nm and are separated by 1 nm. This separation and width of the peaks corresponds to an intracavity etalon of 1.28 mm, corresponding to the distance between the crystal and the input coupler. Turning the crystal somewhat removes the etalon effect and gives a better view of the spectrum. The spectrum of the turned crystal has a FWHM of 4 nm. The spectrum of the idler wave was not measured since it is located outside of the range of the OSA. The corresponding idler wavelength can however be calculated using Eq.(3.7) to be 3190.8 nm and 3187.2 nm respectively. The broad spectrum is an effect of the longitudinal multi mode nature of the pump beam. The feedback in the resonator is slightly narrowing the spectral gain compared to the OPG. The resonator is, however, not limiting the spectral bandwidth in any other manner. Therefore, the multiple longitudinal modes of the pump beam will be transferred to the generated signal and idler.

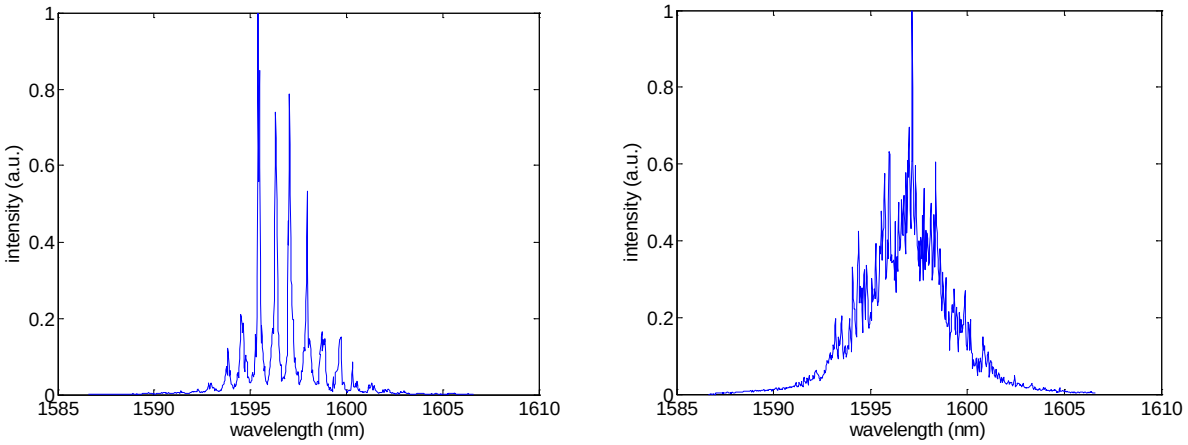

(a) (b)

Figure 4.17: a) Spectrum of the signal in an OPO pumped by a focused Gaussian beam at 50 ˚C. **b)** Spectrum of same OPO with the crystal slightly turned.

A lens with 100 mm focal length of was used to focus the signal after the separation stage, in order to measure the M^2 of the signal. This was measured using the knife-edge method and Eq.(2.6) was then fitted to measured data. Figs. 4.18 display the measured data and the fitting plots. M^2_{horiz}=2 and M^2_{vert}=2.2 were obtained from the fitting. This beam has increased spatial coherence compared to the signal generated in the Gaussian pumped OPG. The spatial coherence is also improved compared to the pump beam. This suggests the presence of a resonator, which provides feedback for the signal, limits possible high gain interactions and controls how the transverse mode of the signal can build up, and hence controls the spatial coherence. In a resonator consisting of two flat mirrors the beam quality factor, M^2, is essentially determined by the beam radius of the pump wave and the length of the resonator. A small misalignment of a mirror will, however, significantly deteriorate the spatial coherence by providing gain for noncollinear processes.

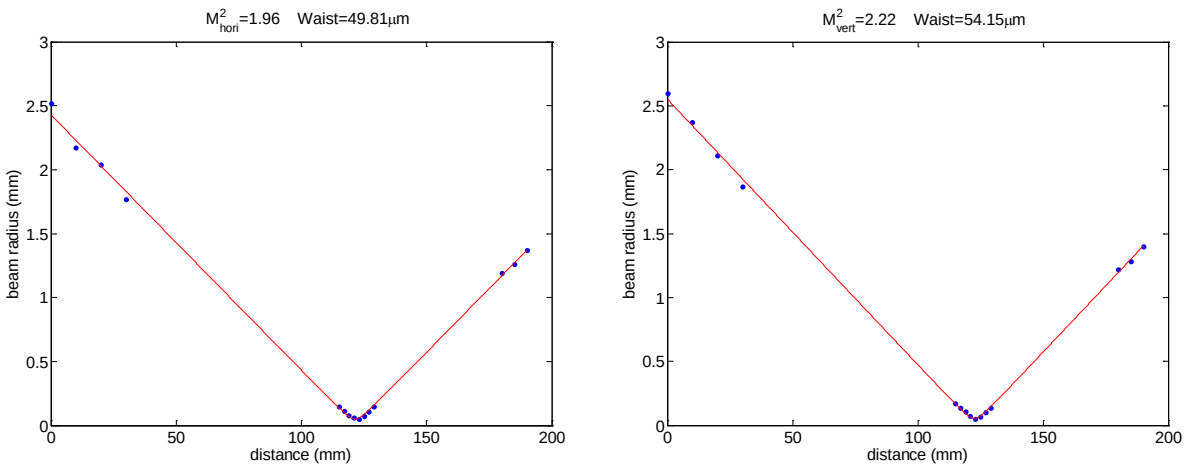

(a) (b)

Figure 4.18: Measured beam radii at several distances from the lens are shown by blue point and the fitting of the measured data to Eq.(2.6) is shown by the red line. The right graph **a)** shows the horizontal measurements and the left graph **b)** the vertical measurements.

4.2.4 Pumping of OPO with a Bessel beam

In the final setup an OPO was set up to be pumped by a beam with a radial Bessel distributed intensity. A schematic figure of the setup is shown in Fig. 4.19. The transverse Bessel intensity was created with an axicon with the prism angle α=1˚, similar to the previous Bessel pumped OPG. The resonator makes it possible to promote one of the two possible processes with high gain and thereby select only one signal and idler pair. The maximum pump energy is limited to 2.4 mJ. The crystal was placed along the focal line of the axicon at a distance of approximately 80 mm. The crystal rested on a copper block and its temperature was controlled and kept at 60˚C.

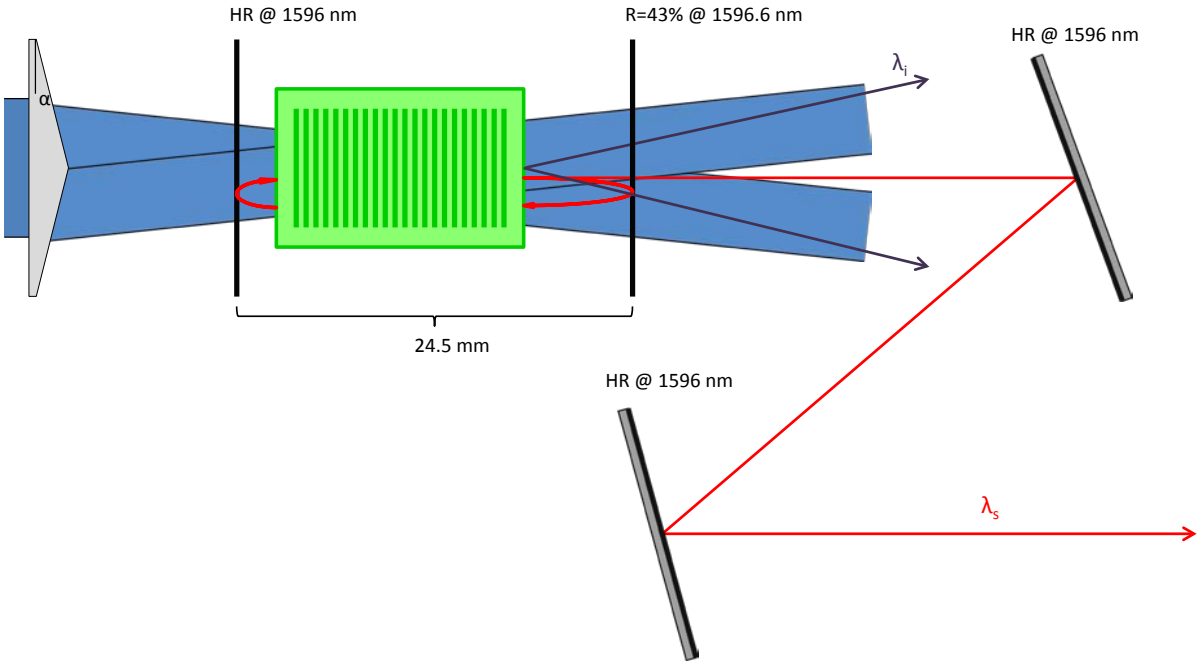

Figure 4.19: Sketch of the setup with blue, red and violet lines representing the pump, signal and idler. The length of the cavity was 24.5 mm.

The efficiency of the OPO is depicted in Fig. 4.20a and the output power of the signal wave is depicted in Fig. 4.20b. The threshold of the parametric process is at 0.6 mJ of input pulse energy. The output power of the signal wavelength increases almost linearly with the input power. The pump depletion and the efficiency increase first with rather steep slopes, and then start saturating as pump powers increase. Neither the efficiency nor the pump depletion shows any sign on decreasing after the maximum values are reached. The curves for the depleted pump and the efficiency follow each other rather closely, indicating that majority of the depleted pump is used in the desired process and that the losses are not so significant. The small losses compared to the Gaussian pumped OPO, confirms the theory that cascaded processes are depleting the measured signal wave. These processes can only take place when the interacting waves are co-propagating, that is, when collinear phase matching is being used and the idler wave is seeding the second parametric process. When employing noncollinear phase matching, these cascaded processes are not present since all interacting waves are propagating in various directions. These losses are mainly due to parasitic processes and

scattering in the cavity. The efficiency of the OPO is 21% at approximately 3 times above threshold and the maximum output energy of the signal is 0.32 mJ per pulse. The resonator which is present and provides feedback for the signal wave yields an increase in efficiency, but also ultimately limits the efficiency of the process at the same time. The efficiency can be optimized for certain power ranges by adjusting the output coupling and the crystal length. Ultimately, it is the length of the nonlinear crystal that affects the efficiency of the process, since it determines the starting point of the nonlinear process. For a long interaction length within the crystal more pump energy can be converted.

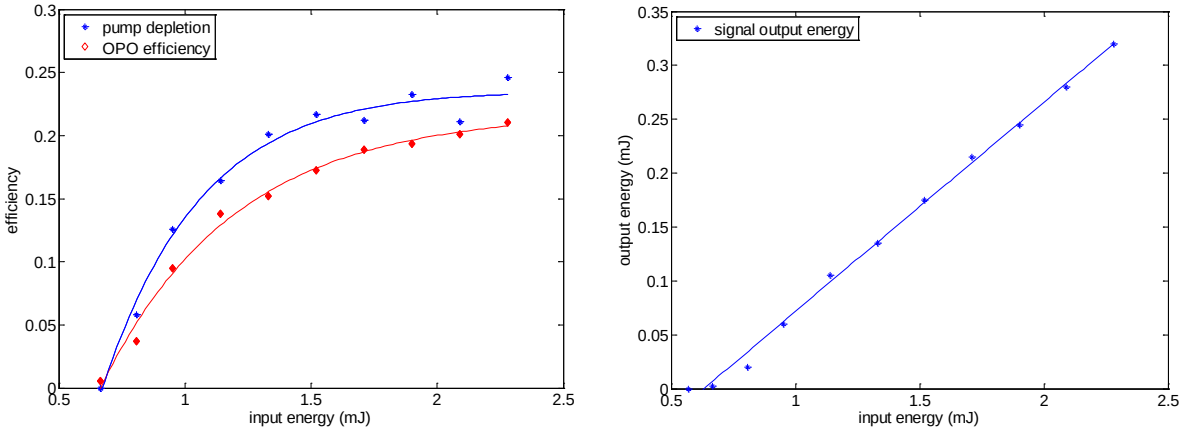

(a) (b)

Figure 4.20: a) Efficiency of the parametric process and depletion of the pump. **b)** The output power of the signal wave

Fig.4.21 shows the spectrum of the OPO at 60˚C, since the desired wavelengths were obtained at this temperature, which was recorded with an OSA. The central peak of the spectrum is located at 1596.5 nm and has a full-width half-maximum (FWHM) bandwidth of 0.2 nm, corresponding to 24 GHz. The corresponding idler wavelength 3190 nm, which is calculated using Eq(3.7). The spectrum of the idler was not measured since it is outside the measureable range of the OSA. The narrow central peak in the signal spectrum shows that the process has a narrow bandwidth, and hence has good temporal coherence. The temporal coherence is an effect of pumping with a transverse Bessel distribution. The phase-matching is noncollinear and makes it possible to promote one single wavelength of the signal since back conversion and the associated spectral broadening is limited. More important is the interference pattern that creates the Bessel beam, provides an automatic selectivity of the spatially coherent wave vectors in the pump beam. The coherence of these wave vectors will be transferred to the signal wave, and therefore generating a highly coherent signal. This effect is, however, only present with when a resonator is used that provides feedback for the signal wave, and by that determines which high gain phase matching condition will be used. The small side peaks are located about 1 nm from the central peak, which corresponds to a Fabry-Perot cavity of 1.28 mm. The crystal was located about 1.28 mm from the input coupler, and none of the end faces of the crystal are AR-coated. Therefore it seems the small peaks are from an intracavity etalon between the input coupler and the end face of the crystal.

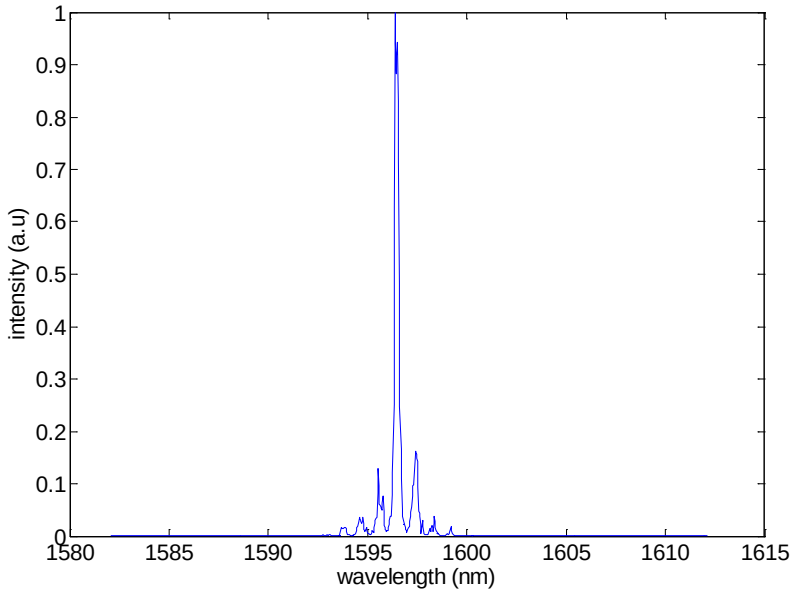

Figure 4.21: Spectrum of the OPO pumped by a Bessel beam taken at 60° C.

After the second mirror in the separation stage, a lens of focal length 100mm was placed in order to measure the beam quality factor, M^2, of the generated signal. The beam radius was measured with the traveling knife-edge method and Eq.(2.6) was then used to fit the measured data to obtain the M^2. The measured beam radii and the fittings are shown in Figs. 4.22 along with the obtained M^2 for both the vertical and the horizontal direction. The fitting of Eq.(2.6) to the experimental data results in M^2_{hori}=1.9 and M^2_{vert}=2.1. This result shows an improvement of the spatial coherence of the generated signal compared to that of the input pump beam, and also to that of the Bessel pumped OPG. This suggests the spatial coherence here is limited by the resonator used.

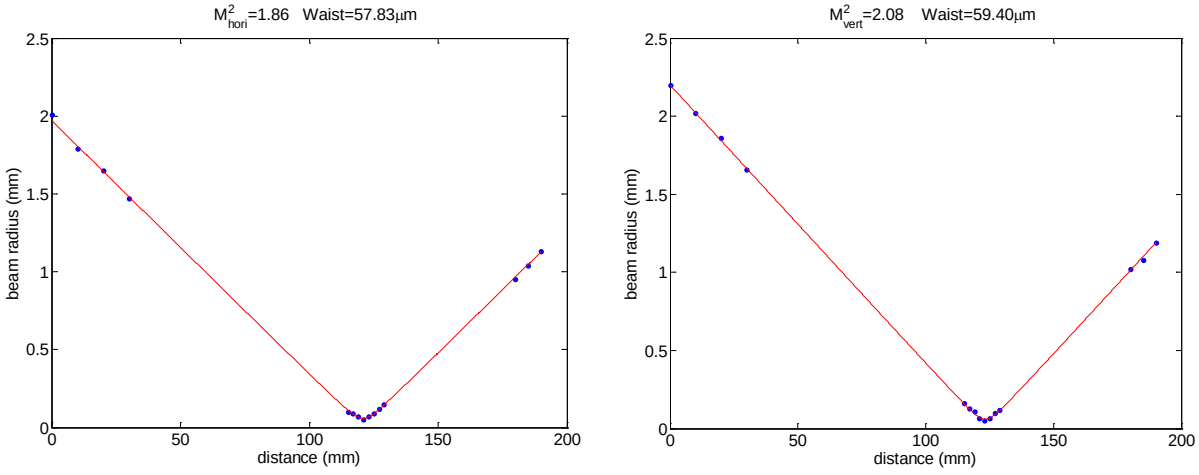

(a) (b)

Figure 4.22: Measured beam radii at several distances from the lens are shown by blue point and the fitting of the measured data to Eq.(2.6) is shown by the red line. The right graph **a)** shows the horizontal measurements and the left graph **b)** the vertical measurements.

4.2.5 Comparison

The four performed experiments can give some insight in how the focusing of the pump beam and how the resonator can affect the nonlinear process. To start this analysis the efficiencies of the two OPO are depicted in Fig. 4.23a and the ones of the two OPG are shown in Fig. 4.23b. The efficiencies are plotted against pump energy above threshold.

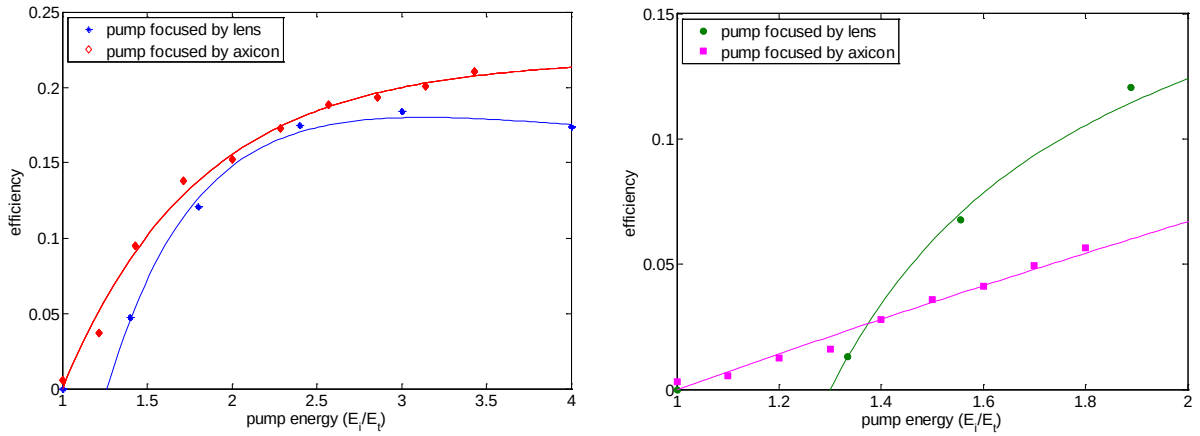

(a) (b)

Figure 4.23*: a)* The efficiencies of the different OPO as a function of power above threshold. The efficiencies follow each other rather closely. **b)** The efficiencies of the two different OPG as a function of power above threshold.

Looking at the OPGs it can be observed that the efficiency of the Gaussian pumped OPG is higher than for that of the Bessel pumped OPG, 6% and 12% respectively about two times above threshold. This is expected from the energy distribution of the Bessel beam. Only a fraction of the total power is contained within the central maximum of the Bessel distributed intensity, while the rest of the power is contained in the rings. Therefore, only the coherent part of the pump beam is used in the process. The noncollinear phase matching, that is an effect of using a Bessel beam, will however increase the threshold of the parametric process. Also, there are two possible high gain processes for the Bessel pumped OPG, and the efficiency is only measured for one of them. The depleted pump is used in both of these processes and this will show as a lower efficiency compared to the Gaussian pumped OPG and significant losses in the process. However, the efficiencies of the two different OPO are rather similar. The curves for the efficiencies follow each other closely and saturate to a value about 20% approximately three times above threshold. The existence of a resonator increases the efficiency of the Bessel pumped process of about three times, compared to the OPG, while the efficiency of the Gaussian pumped process is only increased marginally, compared to the OPG. At first glance, one might expect the efficiency of the Gaussian pumped process to increase more in the existence of a resonator. The efficiency of the Gaussian pumped OPO is decreased due to cascaded energy transfer into the idler wave. Hence, it seems the resonator imposes restrictions on the efficiency in a stronger way than the choice of focusing of the pump beam. This particular resonator seems to limit the efficiency to somewhere around 20%.

The spectra from the different experiments are compared in various ways in Figs. 4.24. To investigate the influence of the different ways of focusing the pump beam, it is of interest to compare the different spectra.

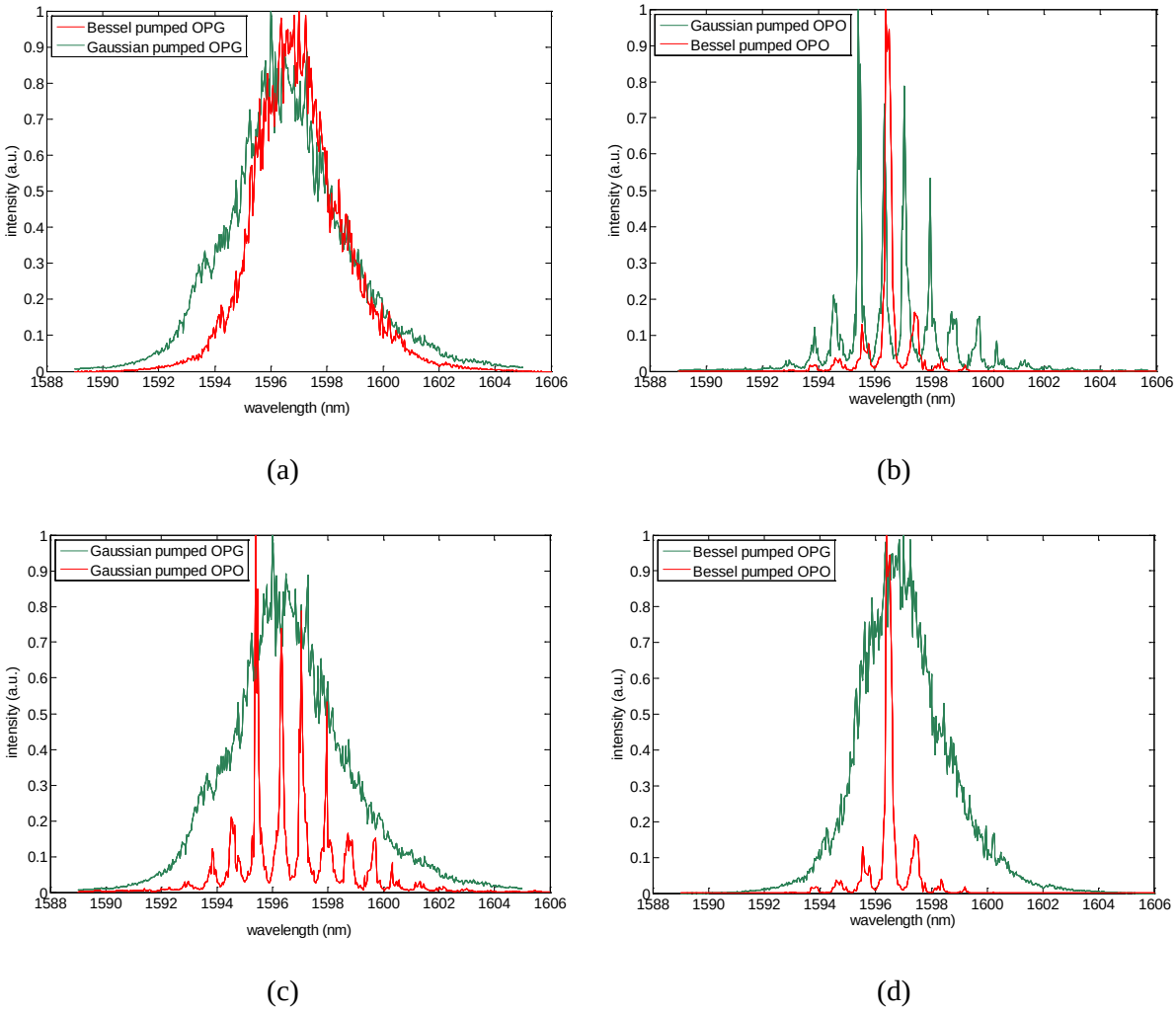

Figure 4.24: a) Spectra of the OPGs . The red spectrum is the OPG with the pump focused by a lens and the green is with the pump focused by an axicon. **b)** Spectra of the OPOs. The red spectrum shows the pump focused by a lens while the green is with the pump focused by an axicon. **c)** Spectra of the OPO (red) and OPG (green) when the pump is focused by an axicon **d)** Spectra of the OPO (red) and OPG (green) when the pump is focused by a lens. All spectra are normalized with respect to themselves.

Fig. 4.24a shows the spectra of the Bessel (green) and Gaussian (red) pumped OPG. The spectrum of the Gaussian pumped OPG is only slightly broader than the spectrum of the Bessel pumped OPG. It could be expected that the difference should be bigger and that the spectrum of the Bessel pumped OPG should be narrower. However, the non-existence of a resonator will cause a broader spectrum since the resonator will impose conditions on the momentum transfer in the process. This can be illustrated in Fig. 4.24d, where the spectra of the Bessel pumped OPG and OPO are shown. The spectrum of the OPO is a lot narrower than the spectrum for the OPG. The spectrum of the OPO looks like a narrower but similar spectrum of the OPG which is modulated by Fabry-Perot transmission. This modulation is an

interference effect due to an intracavity Fabry-Perot etalon between one of the end-faces of the crystal and the input coupler. The same modulation can be seen in the spectrum for the Gaussian pumped OPO when looking at Fig. 4.24b, where the spectra of the two OPO are illustrated. The Gaussian pumped OPO has a few high central peaks and several minor side peaks while the Bessel pumped OPO has one central peak and only a few minor side peaks. The distance between the peaks and the width of the peaks are almost the same in both of the spectra suggesting that it is the intracavity etalon that modulates the spectrum. However, the spectrum of the Gaussian pumped OPO closely resembles that of the Gaussian pumped OPG, modulated by an etalon. This can be seen Figs. 4.24c. The spectrum of the OPO is slightly narrower than that of the OPG, but there is still a pronounced resemblance.

The narrow spectrum of the Bessel pumped OPO is a combined effect of the transverse Bessel distribution and the existence of a resonator. The resonator will narrow the bandwidth due to the multiple passes through the crystal. However, the resonator itself will not impose any other effects except the modulation of the spectrum, which in turn depends on choice of the resonator and the location of the crystal within the resonator. However, the combination of a resonator and focusing the pump beam with an axicon will impose conditions on how the momentum, and energy, can be transferred in the parametric process. The resonator restricts which one of the two high gain noncollinear processes will be operating, and the interference pattern, that creates the Bessel beam, will provide an automatic selection of the spatially coherent wave vectors of the pump beam. The multimode nature of the pump beam, i.e. the pump is characterized by rather broad spectrum and high M^2, will therefore not be visible, since only the part of the beam which is coherent, and therefore creates the interference pattern and focal line, will be used in the nonlinear process. This will cause the generated signal to have a narrow bandwidth and be close to diffraction limited. As an effect, the idler also has a narrow bandwidth and a narrow spread of its ring. The resonator is however a condition for this limitation to take place, since it provides feedback and limits the possible high gain interactions even further. Without the resonator is the spectrum for the Bessel pumped process just as broad as the spectrum of the Gaussian pumped process. Hence, the combination of the resonator and the axicon will drastically improve the temporal coherence of the beam.

Observing the improvement in temporal coherence makes it interesting to look also at the spatial coherence. A good measurement for the spatial coherence is, as previously stated, the beam quality factor, M^2. The various M^2 are listed in Table 1.

	Lens	Axicon
OPG	$M^2 \approx 5$	$M^2 \approx 2.5$
OPO	$M^2 \approx 2$	$M^2 \approx 2$

Table 1: Tabulated values of the averaged M^2 for the different experiments.

As expected from theory [34] does the Gaussian pumped OPG inherit the spatial coherence from the pump beam. An improvement of the M^2 can be observed when the OPG is pumped with a Bessel beam rather than a Gaussian beam. The measured value of the Bessel pumped

OPG is a factor of 2 smaller than the Gaussian pumped process. One might expect the Gaussian pumped OPO to inherit the properties of the pump as well. However, considering both the Bessel pumped and Gaussian pumped OPO, measurements show they have very similar spatial coherence. The big improvement in the spatial coherence when the process is pumped with a Bessel beam, which can be observed in the OPG, is no longer present. Hence, it seems the existence of a resonator is the limiting factor for the spatial coherence, not the method of focusing the pump beam. Ultimately is seems the transversal modes, which exist within the resonator, are the limiting factor for the spatial coherence of the OPO. This suggests the design of the resonator is crucial for high spatial coherence.

Throughout these experiments two flat mirrors where used to create a Fabry-Perot resonator, in which the transversal modes are not Gaussian but rather more irregular transverse patterns. These transverse patterns define how the energy within the resonator will be distributed. It seems this condition on the energy distribution in the resonator is stronger than the method of pumping, and as long as the fundamental mode of the resonator is matched, the choice of focusing will not matter. A decrease the spatial coherence, i.e. a higher M^2, could be obtained by focusing on a bigger area in the crystal so that higher order modes of the resonator will be supported. Therefore, it would be of interest to build an OPO with a resonator with at least one of the mirrors being curved, that is, a stable resonator. By doing so the spatial coherence might be improved further since the transversal modes of that type of resonator are Gaussian.

Ultimately, the performance of the Bessel pumped and the Gaussian pumped OPO are equal except for one property, the temporal coherence. The spectrum of the Bessel pumped OPO is a lot narrower and can be considered better than for the Gaussian pumped OPO. Therefore, the use of the axicon can be used to improve the temporal coherence of an OPO pumped with a multimode laser, while the efficiency and spatial coherence of the process is controlled by the choice of resonator. The efficiency is however also controlled by the length of the crystal. A combination of a stable cavity and a pump beam focused by an axicon would possibly create a signal wave with high spatial and temporal coherence, even when pumped by a beam of low spatial and temporal coherence, making it possible to generate highly coherent beams in the far and mid-infrared part of the spectrum.

5 Discussion and outlook

In Chap. 4.1 an OPO with a stable resonator was built and pumped by a highly coherent beam. The signal and idler inherited the temporal coherence, and the signal also showed a good spatial coherence. However, the spatial coherence was not equal in the vertical and horizontal direction. This was due to the astigmatism of the pump beam, making simultaneous mode matching impossible in both the horizontal and vertical direction. Also, the input coupler is a curved mirror, which will act as a negative lens, changing the measured beam radius and Rayleigh range. Hence, the beam radius will increase due to the input coupling mirror acting as a negative lens, making the area where the crystal is pumped bigger. Both of these factors will decrease the spatial coherence of the generated beam, since they will cause the signal to oscillate in more than one transversal mode.

In Chap. 4.2 the influence of method of focusing the pump beam was investigated. Two sets of experiments were carried out when the pump beam was focused with a lens, with the pump beam retaining its transverse Gaussian intensity distribution and, two sets of experiments were carried out when the pump beam was focused with an axicon, creating a transverse Bessel intensity distribution. The experiments showed that when the pump beam was focused with an axicon the temporal coherence was improved compared to the pump beam used. The spatial coherence and the efficiency of the process, on the other hand were determined by the choice of resonator rather than choice of focusing method. This conclusion raises the question of how the beam quality could be further improved. The resonator used throughout these experiments was a Fabry-Perot etalon with flat mirrors. These resonators does not have pure Gaussian modes, but rather more irregular transverse patterns and suffer from higher power leakage and diffraction losses than stable cavities with well-defined Gaussian modes. Since the transverse modes are not perfectly Gaussian, and the M^2 analysis assumes approximately Gaussian beams, will this show in the measurements as a slightly higher M^2, and hence a slightly worse spatial coherence. The flat-flat Fabry-Perot is, however, convenient to work with since it is easy to align. Therefore, one way of improving the spatial quality would be to build the OPO with a stable resonator. This kind of resonators has well defined transverse Gaussian modes. By appropriately pumping an area smaller than the lowest order transverse mode it is rather easy to obtain a spatially highly coherent beam. When combined with a Bessel distributed pump beam highly coherent beams could be generated, even when a pump beam of poor quality is used. This makes it possible to generate highly coherent beams without the use of a pump source that operates in a single longitudinal and transversal mode.

The main goal of this work is to generate a temporally and spatially highly coherent beam which will be used to seed another parametric process. This is achieved, within the required demands, in two of the setups built. The OPO with a stable resonator which was pumped by a single mode pump source showed a narrow bandwidth of 0.2 nm and a beam quality factor M^2~1.5. The OPO pumped by a conical beam, created from a multimode pump source, shows a bandwidth of 0.2 nm and a beam quality factor, M^2~2. These are two very similar results, despite the two different pump sources used.

The difference in the beam quality factor of the two setups can be accounted for by the use of different types of resonators. As stated in previous analysis the transverse mode patterns of a Fabry-Perot resonator are not perfectly Gaussian but rather more irregular yielding a slightly higher beam quality factor when Gaussian beams are assumed as in the analysis made. To get a more qualitative analysis of the efficiencies and spatial coherence of the different setups the same resonator should be used for both setups. That would make it possible to further investigate the advantages and disadvantages with using a multimode laser to generate highly coherent beams. Multimode Q-switched lasers are in general considered inexpensive, reliable and being able to provide high pulse energies, while lasers operating in single longitudinal and transversal mode are more expensive. The limitations of the spatial coherence and the efficiency when pumping with a conical multimode beam are therefore interesting to be compared to those when pumping with a single mode beam.

When comparing the current setups the spectral bandwidth is of most interest. The OPO pumped by a multimode pump source shows the same spectral bandwidth as the OPO pumped by a single mode pump source, when focused with an axicon creating a conical beam. This shows it is possible to generate a highly coherent signal, or idler, also when using a multimode pump laser. The two setups have the same bandwidth which indicates it is ultimately other things rather than the pump laser that limits how narrow bandwidth can be generated, with proper phase and mode matching. Noncollinear phase matching is a way of generating highly coherent beams since there will be no back conversion or coupling between the generated waves and therefore the range of the wave vectors can be kept very narrow for the desired beam. One option to further investigate this aspect would be to employ noncollinear phase matching combined with a single mode pump source to investigate if the bandwidth becomes even narrower.

The narrow bandwidth generated when pumping with a conical beam is an effect of the non-collinear phase matching, making it possible to generate a signal or idler with a narrow bandwidth. The generated wave which is not propagating along the optical axis (depending on which of signal or idler has the desired wavelength) makes it difficult to use and analyze in a later stage in a cascaded setup. It will, due to the noncollinear phase matching, diverge in a cone with a slightly bigger angle than the one of the pump beam. If it is desirable to use both the signal and idler generated it is therefore of advantage to use the OPO pumped by a single mode pump source. When using collinear phase matching, as in the setup pumped with a single mode beam, there are several possibilities of back conversion and other interactions making the spectrum of the generated beam broadened. With noncollinear phase matching the back conversion and other undesired noncollinear processes, due to couple between the interacting waves, are prevented, keeping the bandwidth of the generated beam narrow.

The Bessel beam used in this work is created with an axicon starting from a multimode laser beam. Since the laser beam is operating in multiple longitudinal modes the coherence length is limited. The limited coherence length imposes restrictions on the transverse Bessel intensity that is created by interference. Due to the multiple oscillating modes in the beam, and hence wavelengths, the interference pattern will not be ideal. The contrast of the interference pattern

will be decreased when the amount of oscillation modes is increasing, and hence, the bandwidth gets broader. It is clear that the noncollinear phase matching is beneficial to generate a signal or idler with a narrow bandwidth. The interference pattern created is however creating a focal line and hence yielding the peak powers required for the parametric process to occur. The transverse Bessel distribution created with the multi mode pump laser is not perfect due to the broad bandwidth of the pump. How this affects the parametric process remains to be assessed.

All spectra of the various OPO in this thesis show narrow peaks due to an intracavity etalon between the crystal and one of the mirrors. This modulation is not necessary a negative effect but needs to be dealt with. One way to take advantage of the etalon effect would be to insert another etalon in the cavity with larger mode spacing. The effects of the narrow peak and the large mode spacing could then be combined. The large mode spacing would then suppress the smaller peaks while supporting the narrow central peak, resulting in a highly coherent wave. This might, however, introduce losses due to scattering and diffraction in the cavity and, slightly worsen the spatial coherence if not accounted for in the design of the resonator. One easy way to make the etalon effect smaller or even remove it completely would be to coat the end faces of the crystal with an anti-reflection coating. If the anti-reflection coating is made for both the signal and pump wave the efficiency of the process could also be increased.

Another way of removing the modulation of the spectrum due to the intracavity etalon would be to build a ring cavity consisting of three or more mirrors. That would mean the signal would be resonating in a traveling wave resonator, rather than a standing wave resonator removing any etalon effects. This would also result in the OPO having a higher threshold and the risk of damaging the crystal due to intense pumping increases. Another disadvantage of using a ring resonator is that it is more difficult to align due to its many degrees of freedom. This kind of resonator might however narrow the bandwidth of the generated signal, increasing the temporal coherence, as well as increasing the spatial coherence when properly matched with the pump beam.

5.1 Future work

The signal and idler waves in the experiment in Chap. 4.1 will later be used to pump a second parametric process to enhance the energy of the idler wave. In this process energy from the signal wave will be used to amplify the idler wave. The idler will thereafter be used to seed an OPO with conversion of radiation from the wavelength of 2μm to a wavelength of 6.4μm, for the MIRSURG project. For the seeded OPO, generating 6.4 μm, is it of importance that the idler possess high spatial and temporal coherence.

It is of interest to further investigate the possibilities of generating a highly coherent beam when pumping the parametric process using a multi mode laser. To get a deeper understanding of the limitations of the noncollinear multi mode pumped OPO is it of interest to compare it with the stable cavity OPO pumped by a single mode laser. This should be done under the same conditions, i.e. with the same resonator to ultimately see how the efficiency of the process and the beam quality factor is affected by the conical beam. If the qualities of the two OPOs are similar this indicates there is a way of generating highly coherent beams in the mid-infrared part the spectrum also with laser that can be considered cheap compared to single mode pump sources. This opens up possibilities for the field of research within generating beams for different applications in the mid- and far-infrared spectrum.

The properties of the multi mode Bessel beam should be studied further than done in this work. It is clear the noncollinear conical beam creates a way of improving the temporal coherence of an OPO when pumped by a multi mode pump source. It is, however, of interest to study the influence on the multi mode nature on the interference pattern created. This could give a deeper understanding on how the interference pattern affects the parametric process. It is also of interest to study the interference pattern when created by a single mode pump source, compared to when it is created with a multi mode pump source. Pumping an OPO with a single mode pump source focused to a conical beam would give further understanding on how the noncollinear phase matching and the interference pattern created affects the process.

References

[1] M.S. Kitai, V.L. Popkov, V.A. Semchischen and A.A. Kharizov *The physics of UV laser cornea ablation*, Quantum Electronics 27, 302 (1991)

[2] Z. Amin, J. J. Donald, A. Masters, R. Kant, A. C. Steger, S. G. Bown and W. R. Lees *Hepatic metastases: interstitial laser photocoagulation with real-time US monitoring and dynamic CT evaluation of treatment*, Radiology 187, 339 (1993)

[3] O.J Beck *The use of the Nd-YAG and the CO_2 laser in neurosurgery*, Neurosurgical Review 3, 261 (1980)

[4] MIRSURG (Mid-Infrared Solid-State Laser Systems for Minimally Invasive Surgery), EU research program, Grant agreement No. 224042

[5] A. Siegmann, *Lasers*, University Science Books (1986)

[6] J. A. Arnaud, W. M. Hubbard, G. D. Mandeville, B. de la Clavière, E. A. Franke, and J. M. Franke, *Technique for fast measurement of Gaussian laser beam parameters*, Appl. Opt. 10, 2775 (1971).

[7] M.A. de Araújo, R. Silva, E. de Lima, D.P. Pereira, and P.C. de Oliveira, *Measurement of Gaussian laser beam radius using the knife-edge technique: improvement on data analysis*, Appl Opt. 48, 393 (2009)

[8] S. De Nicola *Irradiance from an aperture with a truncated J_0 Bessel beam*, Opt. Com.

80, 299 (1991)

[9] D. McGloin and K. Dholakia, *Bessel beams: diffraction in a new light*, Contemporary Physics 46, 15 (2005)

[10] Anna Burvall, *Axicon imaging by scalar diffraction theory*, PhD dissertation, Kungliga Tekniska Högskolan (KTH) (2004)

[11] J.H. McLeod *The Axicon: A New Type of Optical Element*, JOSA 44, 8 (1954)

[12] J. W. Goodman, *Introduction to Fourier Optics, Third Edition*, Roberts & Company Publishers (2005)

[13] E. Hecht, *Optics, Fourth edition*, Pearson Education, Inc. (2002)

[14] P. Franken, A. Hill, C. Peters and G. Weinreich, *Generation of Optical Harmonics*, Phys. Rev. Lett 7, 118 (1961)

[15] T.H. Maiman *Stimulated optical radiation in ruby* Nature 187, 493 (1960)

[16] A.Yariv, *Quantum Electronics, Third Edition*, John Wiley & Sons, Inc (1989)

[17] R.W. Boyd, *Nonlinear Optics*, Academy Press (1992)

[18] G. Hansson, H. Karlsson, S. Wang and F. Laurell, *Transmission Measurements in KTP and Isomrpic Compounds*, Appl. Opt. 39, 5058 (2000)

[19] M.V Pack, D.J. Armstrong and A.V. Smith, *Measurements of the $\chi^{(2)}$tensorns of $KTiOPO_4$, $KTiOAsO_4$, $RbTiOPO_4$ and $RbTiOAsO_4$ crystals*, Appl. Opt. 43, 3319 (2004)

[20] J. A. Armstrong N. Bloembergen, J. Ducuing and P.S Pershan, *Interactions between light waves in a nonlinear dielectric*, Phys. Rev. 127, 1918 (1962)

[21] A.Piskarskas, V.Smilgevičiis, A.Stabinis and V. Vaičaitis, *Spatially cumulative phenomena and output patters in optical parametric oscillators and generators pumped by conical beams*, J. Opt. Soc. 16, 1566 (1999)

[22] A.Piskarskas, V.Smilgevičiis, A.Stabinis and V. Vaičaitis, V. Pasiskevicius, S. Wang, J. Tellefsen and F. Laurell *Noncollinear second-harmonic generation in periodically poled $KTiOPO_4$ excited by the Bessel beam* Opt. Lett. 24. 1053 (1999)

[23] V. Pasiskevicius, H. Karlsson, J.A. Tellefsen, F. Laurell, R. Butkus, A.Piskarskas, V.Smilgevičiis and A.Stabinis *Singly resonant optical parametric oscillator in periodically poled $KTiOPO_4$ pumped by a Bessel beam* Opt Lett 25, 969 (2000)

[24] S.P. Tewari, H. Huang and R.W. Boyd, *Theory of self-phase-matching*, Phys. Rew. A, 51, 2707 (1995)

[25] H. Yoshida, H. Fujita, M. Nakatsuka, M. Yoshimura T. Sasaki, T. Kamimura and K. Yoshida, *Dependences of Laser-Induced Bulk Damage Threshold and Crack Patterns in Several Nonlinear Crystals on Irradiation Detection*, Japanese Journal of Applied Physics 45, 766 (2006)

[26] A. Hildenbrand, F.R. Wagner, J.Y. Natoli, M. Commandré, H. Albrecht and F. Théodore *Laser damage investigation in nonlinear crystals: Study of $KTiOPO_4$ (KTP) and $RbTiOPO_4$ (RTP) crystals*, Proc of SPIE 6998 (2008)

[27] J.M. Manley, H.E. Rowe, *Some General Properties of Nonlinear Elements-Part I. General Energy Relations*, Proceedings of the IRE 44, 904 (1956)

[28] S. Brosnan and R. Byer, *Optical parametric oscillator threshold and linewidth studies*, IEEE J Quantum Electron 15, 415 (1979)

[29] K. Fradkin, A. Arie, A. Skliar and G. Rosenman, *Tunable midinfrared source by difference frequency generation in bulk periodically poled $KTiOPO_4$*, Appl Phys Lett 74, 914 (1999)

[30] K. Kato and E Takaoka, *Sellmeier and termo-optic dispersion formulas in KTP*, Appl Opt. 41, 5040 (2002)

[31] S Emanueli and A. Arie, *Temperature-dependent dispersion equations for $KTiOPO_4$ and $KTiOAsO_4$*, Appl. Opt. 42, 6661 (2003)

[32] A. Zukauskas, N. Thilmann, V. Pasiskevicius, F. Laurell, and C. Canalias, *5 mm thick periodically poled Rb-doped KTP for high energy optical parametric frequency conversion*, Optical Materials Express1, 201 (2011)

[33] http://www.winlase.com/

[34] Björn Jacobsson *Spectral control of lasers and optical parametric oscillators with volume Bragg grating* PhD dissertation, Kungliga Tekniska Högskolan (KTH) (2008)